National University of Science and Technology **POLITEHNICA** Bucharest

Doctoral School of Applied Sciences

PhD thesis - Summary

Atomic Force Microscopy Technique and Temperature and Stress Sensing Techniques along a Telecommunications Optical Fiber – An Innovative Approach

Scientific leader

Prof. Dr.rer.nat. Marian Enăchescu

PhD Student

Jderu Alexandru-Alin

București, 2023

Cuprins

Chapter 1

1. 1. Introduction

The purpose of this PhD thesis is to realize and implement three advanced measurement techniques and three physical devices/equipment associated with these techniques, with applicability in two different scientific fields. The first technique and the first device/equipment described is dedicated to atomic force microscopy, equipment that will be used in scanning the surface profile of the samples of interest, scanning with a resolution capable of visualizing the atoms on the studied surface. The other two techniques and associated equipment described in this thesis are to detect temperature and stress along a telecommunication optical fiber over short (a few meters) and long (over 50km) distances.

The objectives of this doctoral thesis are the following:

i. analysis of the current development stage of these techniques and equipment in terms of performance;
ii. development, implementation and testing of those three devices with similar or improved minimum specifications compared to advanced devices already on the market.

This doctoral thesis is organized into two main parts and consists of six chapters:

The first part of the doctoral thesis consists of Chapters II and III, representing the part of specialized literature and market studies related to those 3 techniques:

- Chapter II: introduces the AFM (Atomic Force Microscope) technique and the performance indicators of AFM systems and is followed by an analysis of existing AFM products on the market.

- Chapter III: presents an introduction to the optical fiber detection technique, followed by an analysis of the current state of BOTDA (Brillouin Optical Time Domain Analysis) and OFDR (Optical Frequency Domain Reflectometry) techniques and equipment's.

The second part of the doctoral thesis consists of Chapters IV, V and VI and represents the original part of this thesis:

- Chapter IV: focuses on the design and development of the assemblies necessary to build the system related to the AFM technique. This chapter concludes with the results obtained with this new system, capable of atomic resolution in air.
- Chapter V: describes the experimental procedures used to implement the detection system related to the BOTDA technique. Following the experiments, the device demonstrates a temperature resolution of 0.2 °C and a deformation resolution of 4 με. At the same time, the obtained results shows a spatial resolution of 1 m supported over a distance of about 100 km.
- Chapter VI: presents the implementation of the device related to the OFDR technique. Using this equipment, a new method of measuring fluid flow through a tube ("Mass flow monitoring") was also developed. The results show a resolution of 1K with a spatial resolution of 5 cm sustained over a distance of several tens of meters.

1. 1. 1. Introduction to Atomic Force Microscopy

Nanotechnology (including nanoscience) is the ability to see and manipulate matter at the nanoscale in order to produce new structures, materials and devices with applications in multiple sectors (e.g. medicine, automotive, aeronautics, energy, etc.), making possible advances outstanding technologies of our days. The era of nanotechnology began once scientists had the right analytical tools, such as the atomic force microscope [1].

Atomic force microscopy (AFM) is one of the most used techniques in the field of nanoscience (in many cases even indispensable), allowing high-resolution (even atomic) imaging of any type of surface, including polymers, ceramics, electronic devices, composites, glass and

biological samples. The AFM technique is capable of evaluating and quantifying multiple types of material properties such as electrical, magnetic, mechanical, etc. simultaneously and in direct correlation with the morphologies of the analyzed surfaces (co-localized analyses) [2, 3, 4].

The indisputable importance of the AFM technique, but also its versatility, led me to consider the design and development (construction) of such a system capable of investigating both extremely small surfaces - down to atomic resolution, and extended surfaces using the same scanning system (piezoelectric tube). However, in order to achieve this, it was imperative to research the techniques and hardware and software solutions already in the market for building such an AFM system.

1. 1. 2. Introduction to fiber optic sensing

The role of optical fibers in detection can be classified according to how the fiber is used. If it is used as a carrier of the physically measured quantity, it is called an extrinsic fiber, and if it translates a quantity into a measurable optical signal, then it is called an intrinsic fiber.

Extrinsic fiber sensors use a fiber optic cable, normally multimode. It is used to transmit a modulated light, either from a fiber-free optical sensor or from an electronic sensor connected to an optical transmitter [5]. Extrinsic sensors can be used in the same way, for example to measure the internal temperature of electrical transformers, where extreme electromagnetic fields make other measurement techniques impossible [5]. Detection techniques using extrinsic fiber optic sensors provide excellent protection of measured signals against noise.

In these time domain detection techniques, a pulse is sent through the fiber and the light reflected by the fiber at each point is analyzed in the time domain (time-of-flight measurement). Different times correspond to different locations along the fiber, and the width of the light pulse determines the final spatial resolution of the technique. There are several techniques in the time domain, which vary depending on the type of scattering that enters the detection.

The devices using these fiber optic sensing techniques have a major impact on recent deployments. The BOTDA technique allows the achievement of stress measurements of the order of με and temperature in the order of °C over distances greater than 100km maintaining a resolution

of 1 m. While the OFDR technique allows the achievement of stress measurements in the order of με and temperature of the order of °C at distances of several tens of meters but with sub-micrometric resolution.

As it can be seen, the indisputable importance of fiber optic detection techniques, but also their versatility, led me to consider the design and development of such a system capable of both long and short range detection. However, for the realization of this device it was imperative to research the current state of development of these techniques (BOTDA and OFDR) but also of the devices already on the market.

1. 2. References

[1] M. Berger, Nanotechnology: The Future is Tiny, Royal Society of Chemistry, ISBN-10: 1782625267, 2016.

[2] P. W. Peter Eaton, Atomic Force Microscopy, New York: Oxford University Press Inc., ISBN 978–0–19–957045–4 (Hbk.), 2010.

[3] E. Meyer, „Atomic force microscopy," *Progress in Surface Science*, vol. 41, nr. 1, pp. 3-49, 1992.

[4] S. Morita, Roadmap of Scanning Probe Microscopy, Springer, ISSN: 1434-4904, 2007.

[5] Y.-J. Rao, Recent progress in fiber-optic extrinsic Fabry–Perot interferometric sensors, vol. 12, Optical Fiber Technology, 2006, pp. 227-237.

Chapter 2

AFM technique and performance indicators of AFM systems. Research of existing hardware and software solutions on the market for building an AFM system.

2. 1. Introduction

The technique used by the atomic force microscope (AFM) generates a type of microscope with a very high resolution, on the order of fractions of a nanometer (nm), a resolution that is more than 1000 times better than that of an optical microscope [1, 2].

In recent years, due to technological developments aimed at applications based on nanoscale properties in fields such as biology, medicine, materials science and engineering, electronics and optoelectronics, the need to develop equipment that uses this technique and is able to provide information has grown considerably at this level.

Based on this study, the software and hardware models that allow the measurement and analysis of the signals generated by the AFM technique were successfully defined and identified. Also, a series of components and elements were identified in which notes of originality can be inserted that can be implemented in the construction of the system, such as a measuring head with an original innovative design, new electronic control and measurement modules, the software platform with user-friendly, adaptable interface for data acquisition and post-processing.

2. 2. Description of the AFM technique

The principle diagram of this device used in the atomic force measurement technique is shown in Fig. 2. 1 and has as its main element a cantilever, used to scan the surface of the sample. This element is the one that interacts with the investigated surfaces during the scans. Basically, when the tip is brought close to the surface of the sample, the interaction forces between them (tip-sample) generate the bending/deflection of the cantilever. The degree of bending can be measured using various methods, the most common being the one based on a

laser-photodetector configuration. In this method a laser beam is aligned on the highly reflective side (back) of the cantilever, which is subsequently reflected in a cell with 4 photodiodes (photodetector), the position on the 4 photodiodes allowing the quantification of the cantilever deflection. In the AFM system, another important component is the piezoelectric tube, which is equipped with a support on which the sample we want to investigate is mounted, thus making it possible to move the sample in the X, Y and Z directions, depending, of course, on the surface [2, 3, 4].

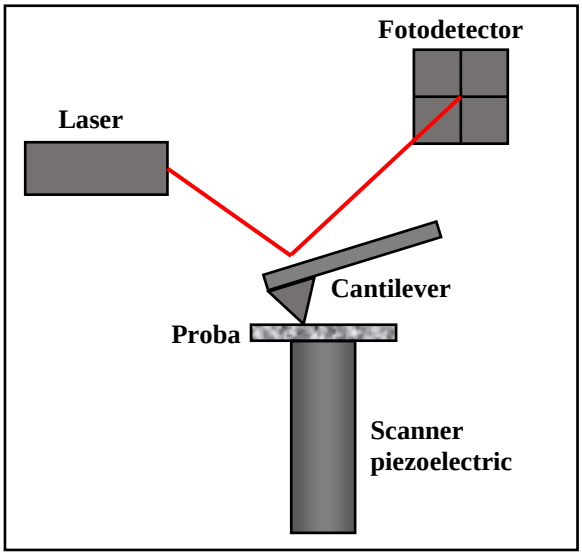

Fig. 2. 1 Schematic representation of the operating principle of an AFM

Such a microscope has several modes of operation, including [5, 6, 7]:

- **Contact mode:** the tip (the cantilever) is brought into contact with the sample and swept over the surface of interest (x, y) keeping the deflection/bending of the cantilever constant through the feedback loop.
- **Non-contact mode:** the tip is oscillated at the resonant frequency of the cantilever, with an adjustable amplitude, generally being a few nanometers. The oscillation amplitude is the feedback signal in this mode. Thus, during a scan, the vertical variations on the surface will generate changes in the oscillation amplitude, the changes being taken over by the controller which will try to keep it constant by adjusting the position of the sample on Z with the help of the piezoelectric tube.
- **Tapping mode:** under normal ambient conditions, most samples form a liquid layer on the surface. Because of this it is very difficult to maintain the tip in non-contact mode so that the forces are detectable and without the tip contacting the sample. In

this mode, the cantilever is oscillated at a frequency below resonance, with an adjustable amplitude, generally 100-200 nm. The piezoelectric tube is used to move the sample in Z in order to maintain a constant peak amplitude. Practically in this mode, the cantilever comes into contact with the sample surface for very short periods of time.

The final objective of this study, on the AFM technique and devices on the market is to design and develop an atomic force microscope capable of working both in contact mode at atomic resolution and in non-contact mode with a vertical resolution of 0.01 nm, capable of imaging small areas, but also extended areas (up to approximately 50x50 μm^2), in multiple environments (ambient conditions, in an environment with controlled humidity, in an environment of inert gases or in a vacuum up to 10^{-4} torr).

2. 3. Performance indicators of AFM

For the effective performance of the above-mentioned study, in the first phase, the parameters that indicates the performance level of the AFM systems were identified.

A first parameter is the **sampling rate**. Sampling rate, in a broad sense, also called sampling frequency defines the number of measurements of a signal in the unit of time [s]. The unit of measurement is Hz, but is sometimes written as S/s (samples/s).

$$f_s = N\left[{}^{kS}/_{S}\right] = N\,[kHz],$$

where f_s is the sampling frequency and N is the number of measurements.

In the case of an AFM system, the sampling rate represents the number of points read per unit of time, as follows:

$$f_{s.p} = N\left[{}^{S}/_{S}\right] = N\,[Hz] = N\left[{}^{points}/_{S}\right]$$

This sampling rate in the case of an AFM system can be represented in several ways using different key quantities. Suppose a 512x512 pixel image is scanned using an AFM. This means that the system finally provides an image consisting of 512 lines, each of these lines having in turn 512 points. This is a first situation in which the sampling rate of an AFM can be calculated. So, to find out the sampling rate of the lines, the following formula can be used:

$$f_{s.l} = \frac{N}{512}\left[{}^{lines}/_{S}\right] = \frac{f_{s.p}}{512}\left[{}^{lines}/_{S}\right],$$

with which the scanning time of a line of 512 points can be identified, which in the example given is 512/N (s).

Also, the sampling rate of the entire image can be calculated, which is another way to use this parameter in AFM. Still considering the same example, the image of 512x512 pixels, the sampling rate can be calculated as follows:

$$f_{s.i} = \frac{N}{512 * 512}\left[{}^{images}/_{s}\right]$$

More specifically, this formula calculates the scan time of a 512x512 pixel image, which is equal to 512*512/N (s).

Resolution is one of the most important parameters that describe the performance of a system in general, this also applies to AFM systems. When discussing data acquisition systems, two types of resolutions can be generally considered. The first type is called "***Peak-to-peak resolution***" or "***noise free resolution***" and can be determined using the noise values given in the datasheet. To determine this resolution, the "*signal-to-noise ratio*" (**SNR**) must first be calculated:

$$SNR = 20\log\left({}^{noise}/_{full-scale\ input}\right)$$

Then, "*Peak-to-peak resolution*" can be found by calculating **SNR** using "*peak noise*" which is equal with 6.6 * "*rms noise*".

$$SNR = 6.02 * N + 1.76 = 20\log\left({}^{noise}/_{full-scale\ input}\right),$$

where N is the accuracy.

For example, according to the datasheet, "*rms noise*" for AD7719 is 1.25µV when the analogic input signal is between +/- 2.56V and has a frequency of 5.35 Hz. Thus we will obtain:

$$20\log\left({}^{6.6 * 1.25E-6}/_{2.56 * 2}\right) = -115.85\ dB,$$

and from here the "*peak-to-peak*" resolution can be calculated as follows:

$$115.85 = 6.02 * N + 1.76 => N = \frac{115.85 - 1.76}{6.02} = 19\ Biti$$

In other words, the "*peak-to-peak"* resolution tells us, given the conditions in the example above, that there will be no jitter in the 19-bit signal.

Another extremely important parameter is **effective resolution**. It is calculated based on the "*rms noise*" parameter, as follows:

$$20\log\left({1.25E-6}/{2.56*2}\right) = -132.25\ dB,$$

thus, achieving an effective resolution of:

$$132.25 = 6.02 * N + 1.76 => N = \frac{132.25 - 1.76}{6.02} = 21.7\ Bits$$

In a simplistic way, the effective resolution shows, in the example considered here, that 21.7 bits will have jitter. Basically, the "*peak-to-peak*" resolution is a better or useful indicator of a system's performance, because it indicates the limit of the number of bits that can be worked on without fluctuations.

It should be noted that AFM system manufacturers may use different methods to calculate these resolutions. The method shown above is used by www.analog.com and is presented for information purposes to show the difference between the two types of resolutions.

2. 4. Study of the existing AFM products in the market

This subchapter presents the results of the study carried out to identify and analyze the performance both in terms of hardware and software of the products manufactured by the companies that supply equipment for measuring atomic forces.

Thus, the companies that produce this type of AFM/SPM equipments, have been identified and are as follows: Bruker; Agilent Technologies – California; Asylum Research – California; JPK Instruments – Germania; NanoScience Instruments – US; Nanosurf; WITec; Park Systems – Korea; Advanced Integrated Scanning Tools for Nano Technology (AIST-NT); NT-MDT – Rusia; AFM Workshop – California; RHK Technology; Nanonics – Israel; Veeco – California; ElbaTech – Italia.

All the products of these companies were analyzed both from the point of view of software and hardware performances (at the hardware level the study was focused especially on the electronics part), and the resulting conclusions are presented in detail in the following sections.

2. 5. The study of the components used as a starting point for the construction of the AFM equipment

As a starting point for the construction of the new atomic force microscope, the "Home built" AFM microscope is used, which was completely built in the laboratory. Based on the

technical data of this equipment, the corresponding performance specifications could be extracted.

Also presented in this chapter is the acquisition board selected as a starting point for the new AFM microscope (NI PXI-7851) along with its specifications and performance.

2. 6. Conclusions

All the information resulting from the conducted study is summarized in the following Table 1.1. Thus, an overview of the performance indicators that define the image acquisition time for the analyzed systems was generated. The information in the table is organized by equipment manufacturer.

Table 1.1 Acquisition time performance of existing AFM systems on the market

Manufacturer	Model	ADC	DAC	Line acquisition time [512pct]	Image acquisition time [512x512pct]	OBS (manufacturer provided information)
BRUKER	Dimension FastScan	-	-	0.016s	8.197s	16Mp image in 8 minutes
	Innova IRIS	100kHz (20bit)	100kHz (20bit)	0.005s	2.65s	Calculated
Agilent	5420	-	-	10.64s	1.52h	Acquisition time
Asylum Research	Cyper S	80MHz (16bit)	40MHz (16bit)	0.0000128 s	0.0065s	Calculated
	MFP 3D	5MHz (16bit)	100kHz (24bit)	0.00512s	2.62s	Calculated
JPK Instruments	NanoOptic	60MHz (16bit)	-	0.0000085	0.0044s	Calculated
	NanoScience / BioScience	60MHz (16bit)	-	0.0000085	0.0044s	Calculated
NanoScience/	Nanite	-	-	0.1024s	52.53s	Calculated

NanoSurf						
WITec	Alpha 300/500	-	-	0.256s	131.58s	Max acquisition speed
Parker	Research branch	500kHz (16bit)	500kHz (16bit)	0.001024s	0.524s	Calculated
	Industrial branch	500kHz (16bit)	500kHz (16bit)	0.001024s	0.524s	Calculated
AIST-NT	SmartSPM 1000	500kHz (18bit)	-	0.001024s	0.524s	Calculated
	CombiScope 1000	500kHz (18bit)	-	0.001024s	0.524s	Calculated
	OmegaScope 1000	500kHz (18bit)	-	0.001024s	0.524s	Calculated
AFM Workshop	Toate	48kHz (14bit)	7kHz (24bit)	0.0731s	37.45s	Calculated
RHK	R9	100MHz (16bit)	100MHz (16bit)	0.00156s	0.8s	Scanning speed 128x128px
	SPM 100	-	-	2s	1020s	Experimental results
Paul Hansma Research	-	-	-	0.001s	0.5s	8 images of 256x256px / s
Softdb	MK2-A810	-	-	0.0034s	1.748s	Calculated
STM	Project	85kSPS	50kHz	0.0102s	5.23s	Calculated
Nanonics	All equipment's	4MHz (18bit)	-	0.000128s	0.06s	Calculated
„Home-built" AFM	-	100kHz (16bit)	200kHz (16bit)	0.05s	26.32s	Calculated
PXI 7851R	-	750kHz (16bit)	1MHz (16bit)	0.000683s	0.35s	Calculated

Calculated refers to the fact that the manufacturer does not specify how long an acquisition takes. The time was calculated according to the data sheet, using the specifications of the slowest component in the system configuration. In reality (experiments), it may be slower.

The final objective of this study aims to design and develop an atomic force microscope with multiple original elements (measurement head with a new design, new electronic modules, new software platform, etc.) capable of working both in contact mode at atomic resolution , as well as in non-contact mode with a vertical resolution of 0.01 nm, capable of imaging small areas, but also extended areas (up to approximately 50x50 μm^2), in multiple environments (ambient conditions, in an environment with controlled humidity, in inert gas medium or vacuum up to 10^{-4} torr).

2. 7. References

[1] P. W. Peter Eaton, Atomic Force Microscopy, New York: Oxford University Press Inc., ISBN 978–0–19–957045–4 (Hbk.), 2010.

[2] K. S. Birdi, Scanning Probe Microscopes, Applications in Science and Technology, eBook ISBN: 9780429214820, CRC Press, 2003.

[3] "Marius Enachescu, D. Schleef, D. Frank Ogletree, Miquel Salmeron," *Physical Review B*, vol. 60, no. 24, 1999.

[4] M. Enachescu, "Nanoscale Effects of Friction, Adhesion and Electrical Conduction in AFM Experiments," in *Atomic Force Microscopy - Imaging, Measuring and Manipulating Surfaces at the Atomic Scale*, InTech, 2012.

[5] M. Berger, Nanotechnology: The Future is Tiny, Royal Society of Chemistry, ISBN-10: 1782625267, 2016.

[6] E. Meyer, "Atomic force microscopy," *Progress in Surface Science,* vol. 41, no. 1, pp. 3-49, 1992.

[7] S. Morita, Roadmap of Scanning Probe Microscopy, Springer, ISSN: 1434-4904, 2007.

Chapter 3

Fiber optic detection techniques and performance indicators. Research of existing hardware and software solutions on the market for detection systems using telecommunication optical fibers as sensors.

3. 1. Introduction to fiber optic detection

The role of optical fibers in the distributed sensing technique can be classified according to the way in which the fiber is used. If it is used as a carrier of the physically measured quantity, it is called an extrinsic fiber, and if it translates a quantity into a measurable optical signal, then it is called an intrinsic fiber.

The technique using extrinsic fiber sensors uses a fiber optic cable, normally a multimode one. It is used to transmit a modulated light, either from a fiber-free optical sensor or from an electronic sensor connected to an optical transmitter [1]. A major advantage of extrinsic sensors is their ability to reach inaccessible places. They are used to measure vibration, rotation, displacement, speed, acceleration, torque and temperature [2].

In the technique using intrinsic fiber optic sensors, the optical fiber itself functions as the sensing element. The structure of an optical fiber generally consists of an elongated cylindrical shape with a Ge-doped SiO_2 core with a refractive index of about 1.54 embedded in a lower IR glass covered with protective plastic layers, Fig. 3. 1. a. In Fig. 3. 1. B is presented how such a simple system can be modeled to work as a distributed sensing mechanism.

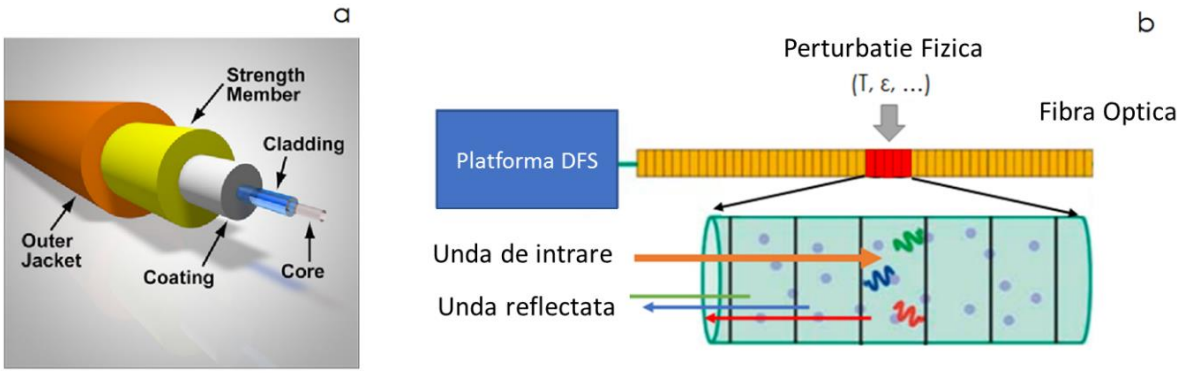

Fig. 3. 1 a). Optical fiber geometry [3]. b). The working principle of a fiber distributed detection system. A fiber can be modeled as a sequence of adjacent sections.

When some physical event occurs in one of these imaginary fiber sections, light is scattered in that section with a slightly perturbed frequency, phase, or amplitude. Scattered light is detected by a DFS (Distributed Fiber Sensing) platform, which can individualize the location of the event along the length of the fiber. The three main scattering modes in the fiber are associated with different light-matter interaction mechanisms (Fig. 3. 2), such as elastic scattering (Rayleigh), photon-photon scattering (Brillouin) and inelastic scattering (Raman).

The anti-Stokes Raman components can be used to obtain temperature measurements, while strain and temperature induce spectral changes in Rayleigh backscattering. Brillouin scattering is sensitive to both strain and temperature, and has the ability to measure/detect very long-range scattering technologies up to 100 km [3].

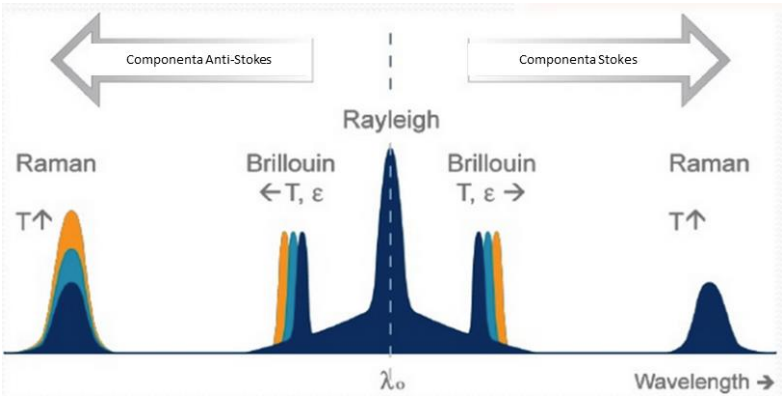

Fig. 3. 2 Scattering processes used in fiber sensing applications.

The indisputable importance of fiber optic detection techniques, but also their versatility, led me to consider the design and development of such a system capable of both long and short range detection. However, in order to achieve this, it was imperative to research the current state of development of these techniques (BOTDA and OFDR) used in building such a system. The main purpose of this study aims to define and identify the operating principles of BOTDA (Brillouin Optical Time Domain Analysis) and OFDR (Optical Frequency Domain Reflectometry) techniques, the progress made by researchers and engineers in their optimization, but also to identify the current limitations of these techniques.

3. 2. Analysis of the current state for the techniques a) BOTDA and b) OFDR

In time domain detection techniques, a pulse is sent through the fiber and the light reflected by the fiber at each point is analyzed in the time domain (time-of-flight measurement). The different times correspond to different locations along the fiber, and the width of the light pulse determines the final spatial resolution of the technique.

We limited the research on key technologies, focusing on Brillouin Optical Time Domain Analysis (BOTDA), and Optical Time Domain Phase Analysis and Optical Frequency Domain Reflectometer (OFDR).

3.2.1 Brillouin optical analysis in the time domain (BOTDA)

Stimulated Brillouin Scattering (SBS) is a non-linear inelastic effect of the 3rd order, which in optical domains exchange part of their energy with dielectrics. Fig. 3. 3 shows the fundamental working principle of stimulated Brillouin scattering. In one of the simple quantum hypotheses, the annihilation of a photon of the injected field, called a pump, generates a photon at the Stokes frequency shifted to lower values and a phonon of the corresponding energy, conserving total energy and momentum. On the other hand, the so-called Stokes photon can be created at higher energy also by absorbing a phonon with the corresponding energy and momentum. In a classical hypothesis, SBS is a parametric process between the pump and Stokes through an acoustic wave induced by electrostriction due to the existence of electric fields. This refractive index scatters the pump wave by Bragg diffraction.

In accordance with the conservation of total energy and momentum, the Stokes/anti-Stokes wave turns out to be backscattered from the incident light wave. The difference between the frequencies of incident light and diffuse light is the same BFS (Brillouin Frequency Shift or vB). While BOTDR (Brillouin Scattering and Brillouin Optical Time Domain Reflectometry) is based on spontaneous Brillouin diffusion, BOTDA uses SBS to achieve higher.

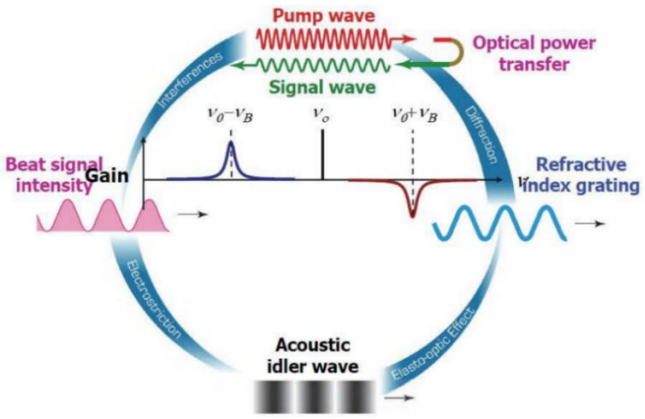

Fig. 3. 3 The physical mechanisms behind SBS [7]

In Fig. 3. 4 a typical BOTDA system is presented. The output signal from a CW laser is split by a 50:50 coupler to generate both the pump and reference signals. An EOM is driven by a pulse generator that is used to generate an amplitude modulated phase reference signal at a high repetition rate in the upper arm of the setup. In the lower arm, another EOM modulates the laser light with a sine wave, which has the same frequency as the BFS and is used to generate the Stokes reference signal. Both the pump and reference signals are generally adjusted using Erbium Doped Fiber Amplifier (EDFA). The reflected Brillouin signal is isolated using a circulating pump and filtered with an FBG (Fiber Bragg grating), which cuts out all spurious harmonics.

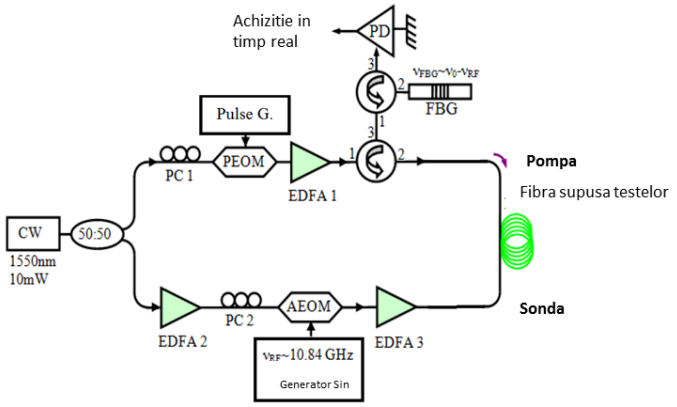

Fig. 3. 4 Typical basic BOTDA configuration [9]

Fig. 3. 5 shows a typical example of SBS reflected by an optical fiber where a point at its end is stressed, a photodetector, a data acquisition and processing system, and SBS analysis.

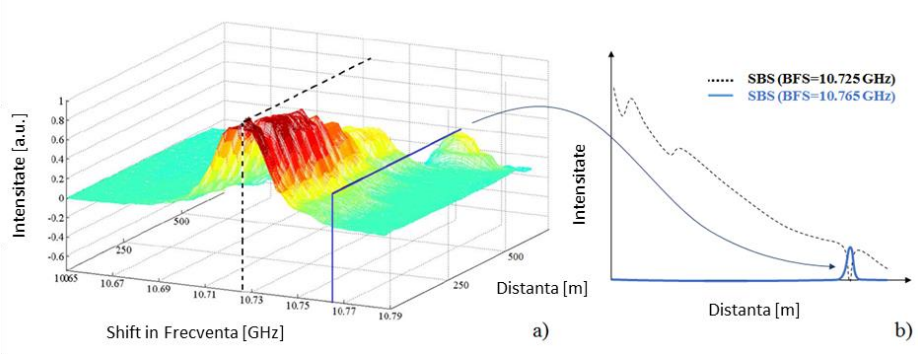

Fig. 3. 5 Frequency – Time/Distance SBS acquisition and analysis (a). Time/Distance domain plot of the same scan over two frequencies (b) [9]

The setup required for the BOTDA technique needs access to both ends of the fiber, as the pump and CW reference must back-propagate into the fiber. This may be considered a limitation in certain situations. Because Brillouin scattering is a polarization-dependent effect, when polarization-maintaining fibers are used, the polarization state can be maintained over a long distance, provided that the initial polarization is oriented either along the fast axis or the slowness of the fiber. When single-mode fibers are used, the polarization states are random along them, due to random fluctuations in the birefringence of the fiber caused by fluctuations in the core shape and non-uniform stress acting on the core, so Brillouin averaging is required over all polarization states.

The configuration using the BOTDA technique is still under development, showing constant progress. Among the solutions are proposed methods for extending the detection limit and improving the spatial resolution.

3.2.2. Optical Reflectometer in the Frequency Domain (OFDR)

All Optical Frequency Domain Reflectometer (OFDR) techniques use Rayleigh scattering to simultaneously interrogate multiple low-frequency low-reflectivity FBG gratings or single fibers, which act as strain and/or temperature sensors along a single optical fiber.

The key benefits of OFDR technology are related to the quasi-continuous wave mode generated by the laser and the narrowband detection of the optical backscattered signal, whereby a significantly higher signal to noise ratio is achieved compared to conventional pulse technology OTDR (Optical Time Domain Reflectometry), or BOTDA. This technical benefit allows the use of affordable semiconductor laser diodes and signal averaging electronics. This is offset by the technical difficulty of measuring scattered Raman light and the complex signal processing due to FFT (Fast Fourier Transformation) calculations with high linearity requirements for electronic components. Although the experimental setup is relatively simple, the algorithms to decipher local temperature and/or strain variations are more complex than those used in most time domain techniques.

OFDR techniques use Rayleigh scattering to simultaneously interrogate several hundred low-reflectivity Bragg gratings (FBGs) that act as strain or temperature sensors along a single optical fiber. The backscattered optical signal interferes with the reflection of the reference light, which serves as a local oscillator, thus resulting in a complex interferogram but with a simple optical scheme (Fig. 3. 6).

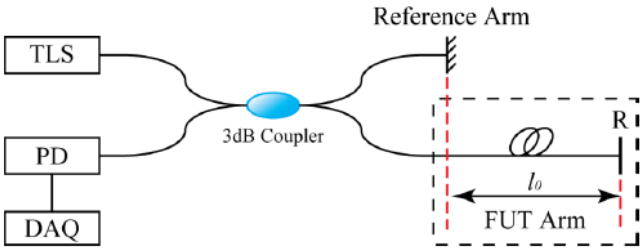

Fig. 3. 6 OFDR schematic [26]

Also, C-OFDR and Kerr Phase Interrogator OFDR can be used as solutions to increase spatial resolution, and have been shown to achieve up to 6 mm resolution over a 3-meter range and 11.2 cm for domains over 151 km. Even though these numbers are impressive, there are other parameters to consider. Other fundamental limitations of OFDR are detection range and detection resolution.

3. 3. Conclusions

A literature review was successfully carried out to understand as precisely as possible the working principles of fiber optic detection techniques, as well as the progress made by researchers and engineers in their development and optimization. The analysis also aimed at evaluating the limitations of fiber optic detection techniques, thus allowing us to identify the optimal configurations for building such systems.

In other words, the limitations of these techniques do not allow the realization of a single optical fiber detection system that is capable of operating both at short and long distances. Thus, in order to have a long-range detection system, namely about 100 km, with a resolution of 1 m, a system will be built using the BOTDA detection technique. The process of developing, testing and implementing the system based on the BOTDA technique will be presented in detail in the next chapter. And for the construction of a detection system that works optimally at small distances, i.e., a maximum of a few tens of meters, but with a resolution of a few µm, we will use the OFDR detection technique. The development, testing and implementation process of the system based on the OFDR technique will be presented in the penultimate chapter.

3. 4. References

[1] Y.-J. Rao, Recent progress in fiber-optic extrinsic Fabry–Perot interferometric sensors, vol. 12, Optical Fiber Technology, 2006, pp. 227-237.

[2] C. R. D. L. F. S. a. F. H. U. Roland, A new fiber optical thermometer and its application for process control in strong electric, magnetic, and electromagnetic fields, vol. 1, Sensor Letters, 2003, pp. 93-98.

[3] E. Udd, „Fiber optic sensors," 1993.

[4] Corning, „Basic Principles of Fiber Optics, Corning Cable Systems.," (2005, 12 Apr). [Interactiv]. Available: www.corningcablesystems.com/web/college/fibertutorial.nsf/ofpara.

[5] J. C. Palais, Fiber optic communications: Prentice Hall Englewood Cliffs, 1988.

[6] J. C. J. a. H. F. Taylor, „"Distributed fiber optic intrusion sensor system for monitoring long perimeters," in Defense and Security," 2005, pp. 692-703.

[7] T. K. a. M. T. T. Horiguchi, „Technique to measure distributed strain in optical fibers," *IEEE Photonics Technology Letters*, vol. 2, pp. 352-354, 1990.

[8] L. T. a. P. A. R. M. Nikles, „Simple distributed fiber sensor based on Brillouin gain spectrum analysis," *Optics letters*, vol. 21, pp. 758-760, 1996.

[9] Y. Mao, „Distributed optical fibre sensing system based on Brillouin scattering," *The Hong Kong Polytechnic University*, 2014.

[10] S. F. Mafang, „Brillouin Echoes for Advanced Distributed Sensing in Optical Fibres," 2011.

[11] L. Thévenaz, „Brillouin distributed time-domain sensing in optical fibers: state of the art and perspectives," *Frontiers of Optoelectronics in China*, vol. 3, pp. 13-21, 2010.

[12] A. D.-L. A. L.-G. J. A.-C. S. M.-L. a. M. G.-H. X. Angulo-Vinuesa, „Rating the limitations and effectiveness of BOTDA range extension techniques," *International Conference on Optical Fibre Sensors (OFS24)*, vol. 4, pp. 96346R-96346R, 2015.

[13] J. W. B. S. S. R. N. L. Z. M. C. A. E. W. a. M. T. A. Voskoboinik, „SBS-based fiber optical sensing using frequency-domain simultaneous tone interrogation," *Journal of lightwave technology*, vol. 29, pp. 1729-1735, 2011.

[14] A. C. R. B. a. L. Z. A. Minardo, „Heterodyne slope-assisted Brillouin optical time-domain analysis for dynamic strain measurements," *Journal of Optics,* vol. 18, p. 025606, 2016.

[15] A. M. a. M. T. ". B. o. t. d. a. f. d. s. Y. Peled, „Optics express," vol. 20, pp. 8584-8591, 2012.

[16] N. H. H. F. K. Y. S. a. K. N. Y. Mizuno, „Ultrahigh-speed distributed Brillouin reflectometry," *Light: Science and Applications,* vol. 5, 2016.

[17] [Interactiv]. Available: http://www.neubrex.com/htm/technology/kouseido_2.htm.

[18] D. J. W. C. N. P. a. D. A. J. V. Lecoeuche, „Transient response in high-resolution Brillouin-based distributed sensing using probe pulses shorter than the acoustic relaxation time," *Optics letters,* vol. 25, pp. 156-158, 2000.

[19] X. B. Y. W. a. L. C. L. Zou, „Coherent probe-pump-based Brillouin sensor for centimeter-crack detection," *Optics letters,* vol. 30, pp. 370-372, 2005.

[20] B. G. C. a. K. B. A. W. Brown, „Dark-pulse Brillouin optical time-domain sensor with 20-mm spatial resolution," *Journal of lightwave technology,* vol. 25, pp. 381-386, 2007.

[21] L. T. a. S. F. Mafang, „Distributed fiber sensing using Brillouin echoes," *19th International Conference on Optical Fibre Sensors,* pp. 70043N-70043N-4, 2008.

[22] K. I. a. J. N. J. Nakayama, „Optical fiber fault locator by the step frequency method," *Applied optics,* vol. 26, pp. 440-443, 1987.

[23] M. N. a. S. A. N. D. W. Dolfi, „ 5-mm-resolution optical-frequency-domain reflectometry using a coded phase-reversal modulator," *Optics letters,* vol. 13, pp. 678-680, 1988.

[24] M. W. V. M. P. M. K. Yuksel, „Optical frequency domain reflectometry: A review," în *11th International Conference on Transparent Optical Networks*, 2009.

[25] R. MacDonald, „Frequency domain optical reflectometer," *Applied optics,* vol. 20, pp. 1840-1844, 1981.

[26] J. Song, „Optical Frequency Domain Reflectometry: Sensing Range Extension and Enhanced Temperature Sensitivity.," *Université d'Ottawa/University of Ottawa,* 2014.

Chapter 4:

Realization of the new AFM system and its successfully demonstrated performance in the laboratory

4. 1. Introduction

The technique of atomic force microscopy (AFM) generates a type of microscope with a very high resolution, of the order of fractions of nm, a resolution that is 1000 times better than that of optical microscopes [1, 2].

The operation scheme of this device that uses the technique of atomic forces is presented in Fig. 4. 1 and it was described in detail in chapter two.

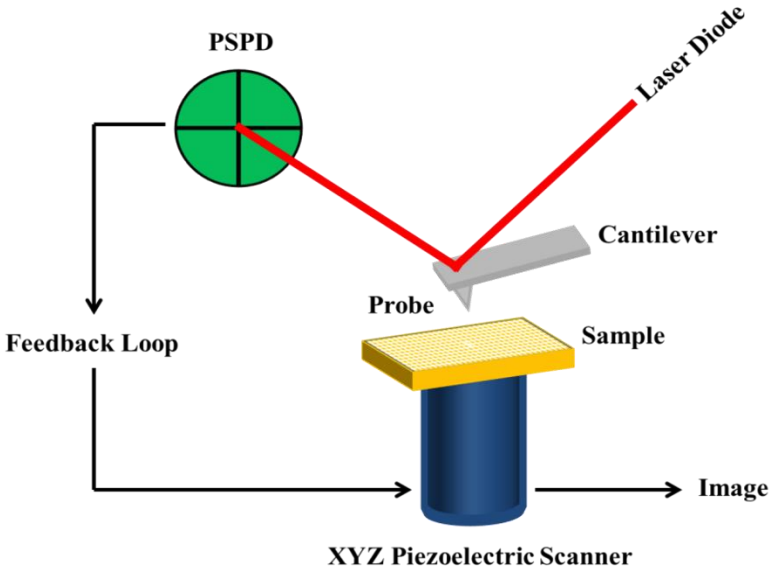

Fig. 4. 1 Experimental configuration for and AFM system

The final objective of this thesis aims to design and develop an atomic force microscope with multiple elements of originality (measurement head with a new design, new electronic

modules, new software platform, etc.) capable of working both in contact mode at atomic resolution , as well as in non-contact mode with a vertical resolution of 0.01 nm, capable of imaging small areas, but also extended areas (up to approximately 50x50 μm^2), in multiple environments (ambient conditions, in an environment with controlled humidity, in inert gas medium or vacuum up to 10^{-4}torr).

4. 2. The design and development of the assemblies required to build the AFM system

The Atomic Force Microscope (AFM) is a complex characterization equipment being made by assembling different components, which is why, in order to increase efficiency in the process of building such a system, a division of design, development and/or assembly activities of the necessary elements is extremely useful. Thus, the construction of the atomic force microscope (AFM), which is the subject of this doctoral thesis, was achieved by grouping the necessary subassemblies into two main categories. In the first part, the optical and mechanical elements were designed and developed, and in the second part, the control electronics of the system were designed and implemented.

4.2.1. Optical and mechanical components

The elements that make up the optical and mechanical subassemblies, necessary for the construction of the AFM system and which must be designed, developed and/or assembled, are the following: (1) atomic force microscope base; (2) piezoelectric scanning system; (3) measuring head and (4) optical detection system. Thus the resulting system can be observed in Fig. 4. 2.

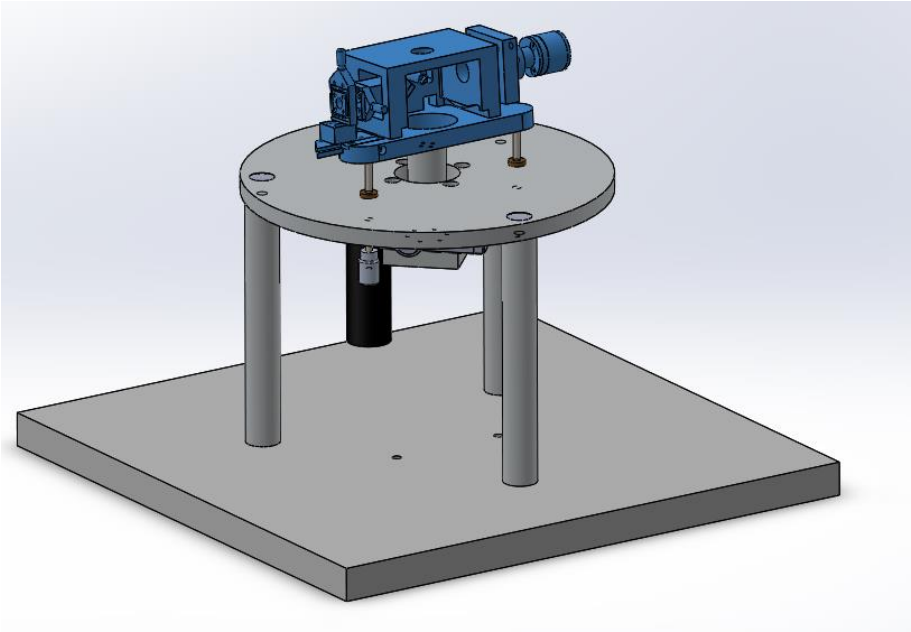

Fig. 4. 2 Completed AFM system

4.2.2. Electronics (control unit) of the AFM system

The atomic force microscope is divided into three major sections: (1) the readout head, (2) the central unit, and (3) the digital data acquisition, processing, and control unit.

From an electronic point of view, the atomic force microscope is composed of the following component blocks:

1. The preamplifier module;
2. The interconnection module A;
3. The interconnection module B;
4. The interconnection module C;
5. Power source;
6. High voltage amplifier.

The preamplifier module ensures the amplification of the signal captured by the four-quadrant photodetector, powered by the laser diode, and performs the mathematical operations between the 4 amplified channels to provide the Normal, Lateral and Total signal information, signals useful in generating images of the scanned surface.

Interconnect module A provides the connection between the digital acquisition and control block, the power supply and the rest of the system component blocks. Contains no active ingredients.

The interconnect module B provides the connection between the preamplifier, the piezoelectric tube assembly, the interconnect module A, the touch screen, the output of the high voltage amplifiers and the rest of the system. It contains an amplification block for the 4 signals received from the preamplifier, an amplification block for the tip excitation piezoelectric element, a motor control block that controls the approach and distance of the sample tip, and a voltage switching block applied to sections of the piezoelectric tube.

Interconnection module C provides the connection of the linearization capacitors between the high voltage amplifiers and interconnection module B. This module contains no active electronic components.

The power supply is a linear, low-noise, multi-section power supply with a total power of 450W, which provides power to all components of the SPFM system. It provides the following stabilized voltages ±5V, ±12V, ±480V and an un-stabilized voltage of 12V. In the composition of the power supply, a module for automatic disconnection of the high voltage was introduced when a high temperature is detected at the level of the cooling radiators.

The high-voltage amplifier was designed to be able to provide a maximum voltage of ±450V, at a minimum current of 100mA, to be able to satisfy the needs of moving the piezoceramic tube, in the linearization configuration by the method of inserting a capacitor.

The amplifier was made in MOS-FET technology for the final and pre-final stages, due to the very high voltages at which these stages have to work.

4. 3. Conclusions

The optical and mechanical elements as well as the control electronics of the system have been successfully designed, developed and assembled, thus building a functional atomic force microscope.

The functionality of the AFM system built "in house" was also tested experimentally. For this purpose, a special calibration grid for AFM systems was selected, namely TGZ01, which has

a step (z) of 20 nm, not presenting a very high effort for the feedback loop of the system. The obtained topographical images are presented in Fig. 4. 3 in both 2D and 3D projection.

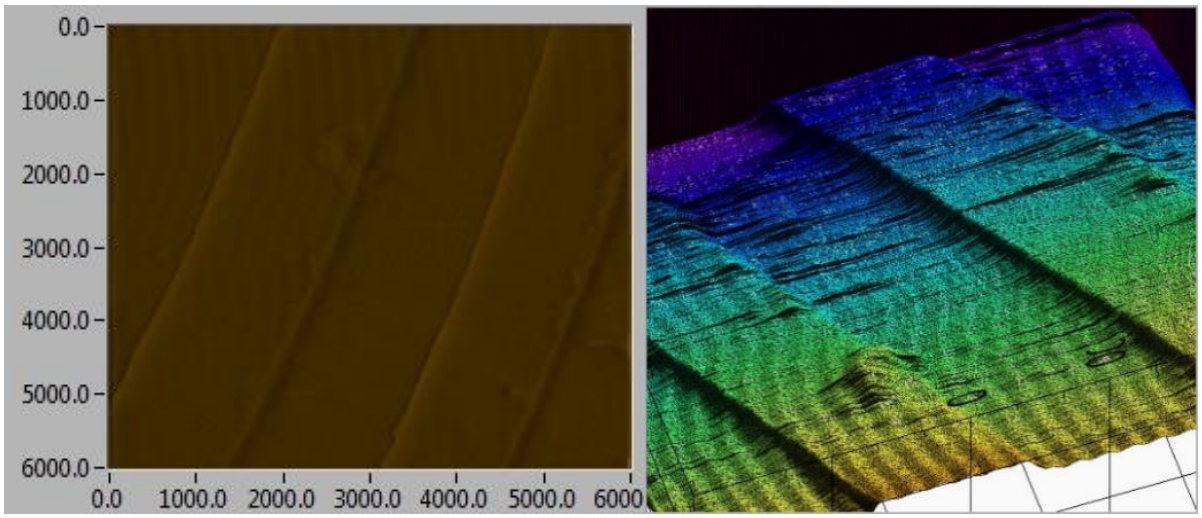

Fig. 4. 3 Topography image for the TGZ01 calibration grid; on the left 2D profile and on the right 3D profile

By successfully scanning the TGZ01 grid, the functionality of the system was demonstrated. So, in order to test the system in more difficult conditions, it was decided to scan another calibration grid, namely TGZ02, which forces the limits of the system, which has a step (on z) of 110 nm. As can be seen in Fig. 4. 4 and Fig. 4. 5, the system is capable of scanning large areas (tens of microns) and detecting fairly large height variations on Z, i.e. topographical properties.

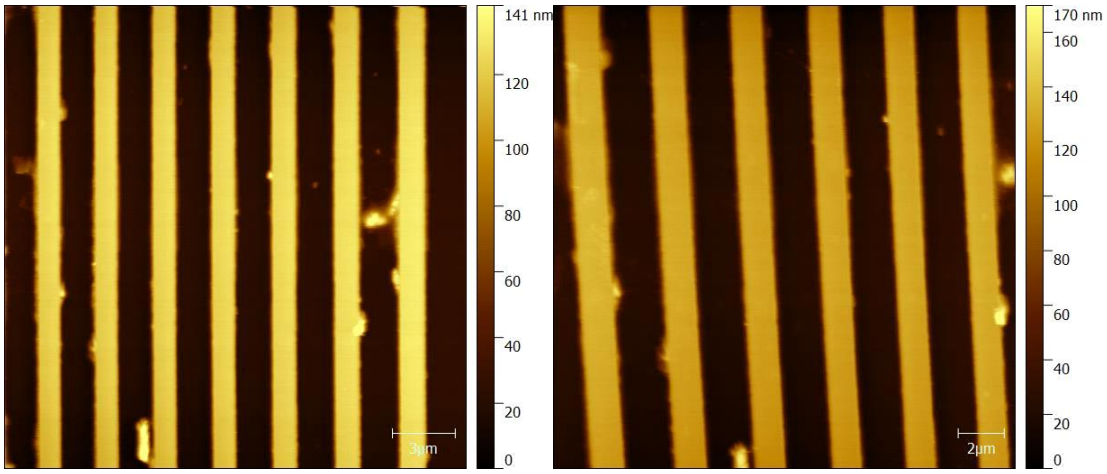

Fig. 4. 4 Images obtained on TGZ02

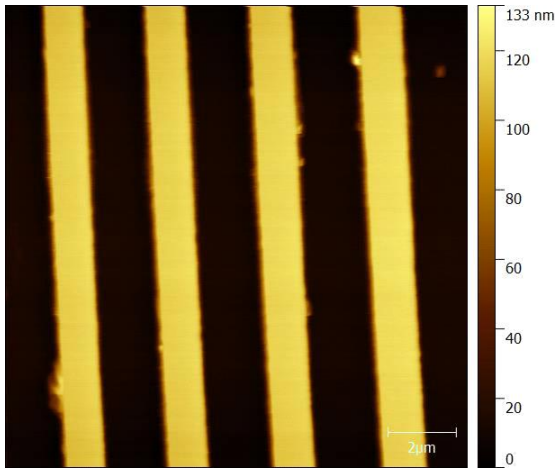

Fig. 4. 5 Magnification of an area on TGZ02

Based on the studies carried out on the two calibration grids, TGZ01 and TGZ02, it can be concluded that the built AFM system is able to record morphological properties with notable height variations without difficulties.

To test the limits of the system, i.e. the most sensitive part, namely scanning at very small dimensions in an attempt to obtain images at atomic resolution under ambient conditions (room temperature, humidity RH 55%), a freshly uniform cleaved mica sample was used. The results obtained are promising, highlighting the atoms on the surface of the mica, including their distribution in the unit cell corresponding to the mica, as can be seen in Fig. 4. 6.

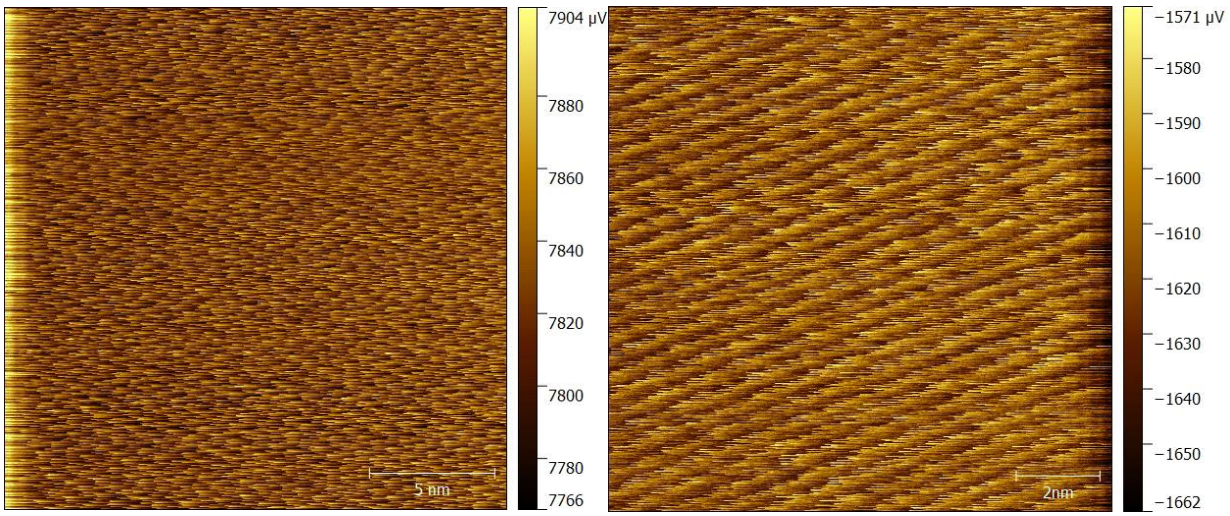

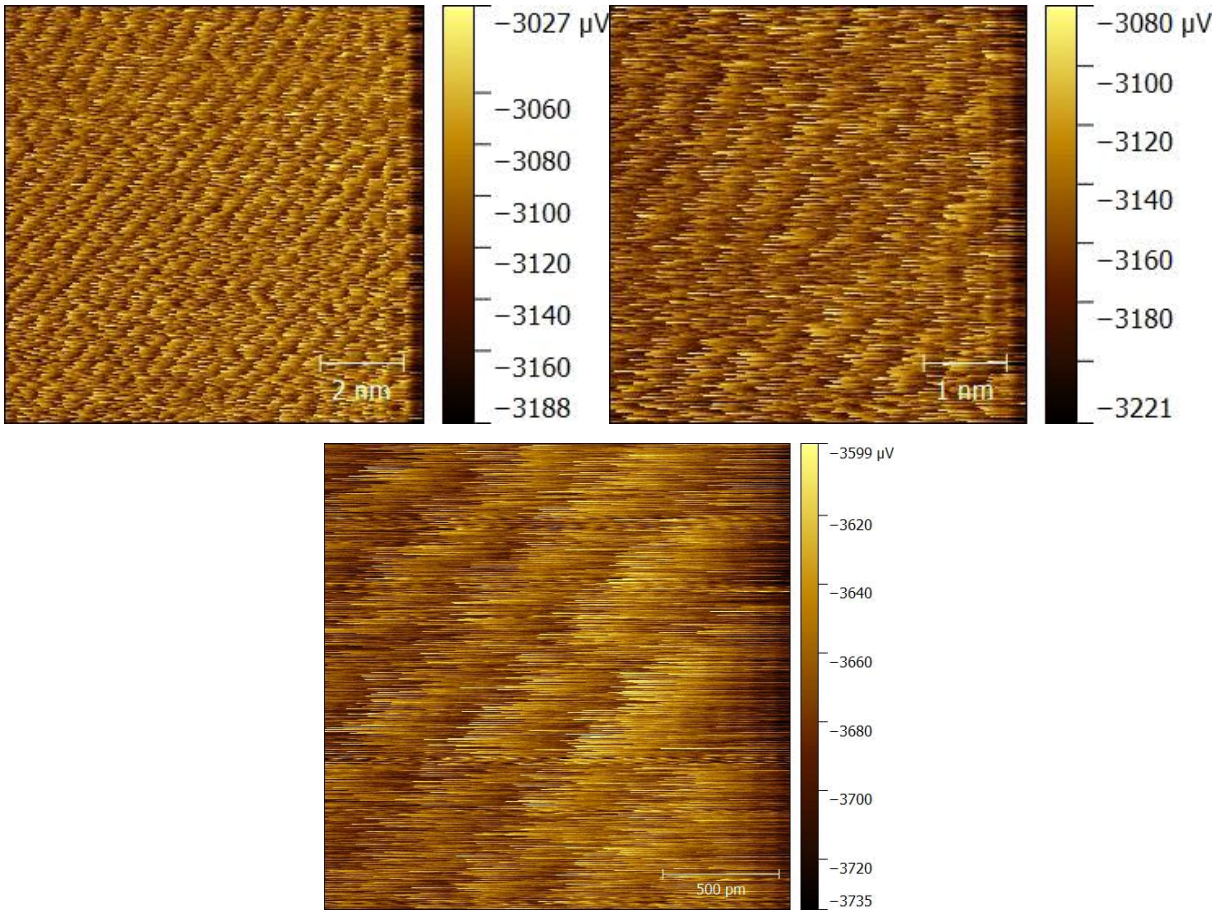

Fig. 4. 6 Atomic resolution achieved with the atomic force microscope built "in house"

The fact that the constructed AFM system is capable of atomic resolution imaging demonstrates its ability to achieve the highest resolutions in all common AFM modes, such as AFM topography, AFM-conductive, etc.

4. 4. References

[1] K. S. Birdi, Scanning Probe Microscopes, Applications in Science and Technology, eBook ISBN: 9780429214820, CRC Press, 2003.

[2] P. W. Peter Eaton, Atomic Force Microscopy, New York: Oxford University Press Inc., ISBN 978–0–19–957045–4 (Hbk.), 2010.

Chapter 5

Realization of a long-range detection system (BOTDA technique). Performance in the laboratory with the developed system

5. 1. Introduction

In intrinsic fiber optic sensors in the distributed sensing technique, the optical fiber itself functions as the sensing element. The structure of an optical fiber generally consists of an elongated cylindrical shape, Ge-doped SiO2 core with a refractive index of about 1.54, embedded in a lower IR glass, covered with protective plastic layers, see Fig. 5. 1 a. Fig. 5. 1 b shows how such a simple system that can be modeled to work with a distributed detection mechanism [1, 2, 3].

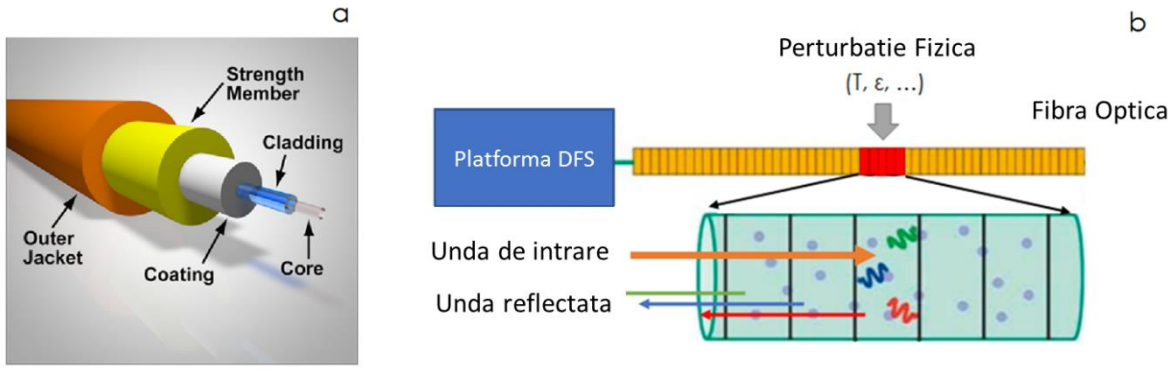

Fig. 5. 1 a). The geometry of an optical fiber, with the outer jacket [4]. b). The working principle of a generic DFS system. A fiber can be modeled as a sequence of adjacent sections. A physical perturbation (e.g. temperature change, strain, acoustic wave, etc.) changes the local state of the fiber, thus resulting in a change in the reflected light wave

When some physical event occurs in one of these imaginary fiber sections, light is scattered in that section with a slightly perturbed frequency, phase, or amplitude. Scattered light is detected by a DFS platform, which can individualize the location of the event along the length of the fiber.

A typical system used to implement BOTDA is shown in Fig. 5. 2 and the operating principle was detailed in chapter three.

The decay of the signal found on the distance (time) axis is due to the loss of signal energy along the fiber. Energy is dissipated at a difference frequency, which is linearly related to the amount of strain or temperature applied to that point (Fig. 5. 3).

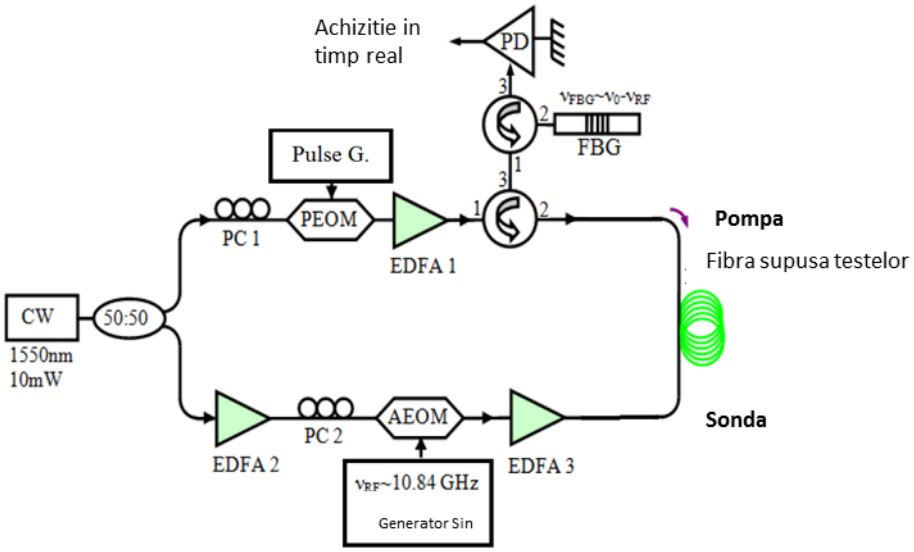

Fig. 5. 2 Typical basic BOTDA configuration [6]

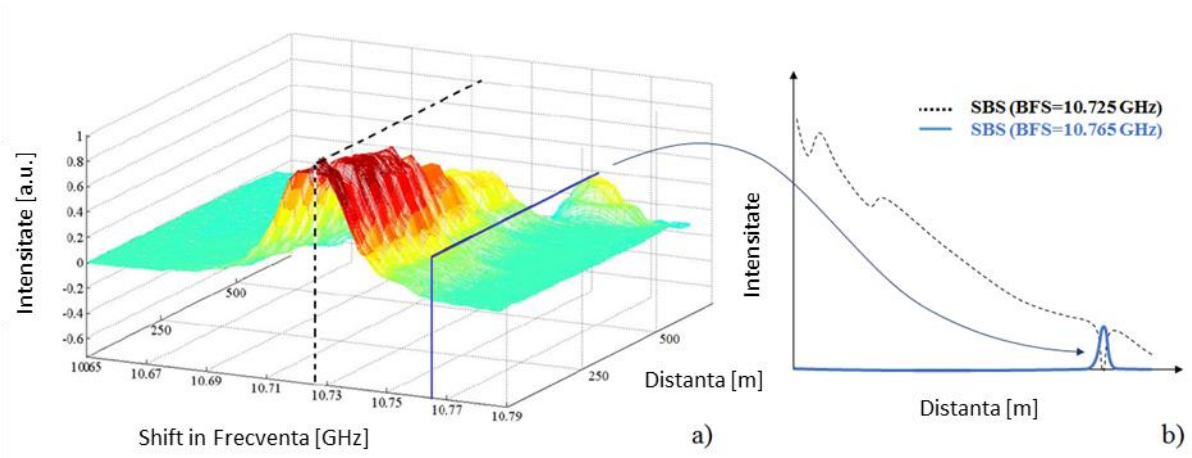

Fig. 5. 3 Frequency – Time/Distance Domain SBS acquisition and analysis (a). Time/Distance domain plot of the same scan over two differences (b) [6]

The configuration using the BOTDA technique requires access to both ends of the fiber, because the CW (continuous wave laser) pump and reference pulse must counter-propagate in the detection fiber. This may be considered a limitation in certain situations.

5. 2. Implementation of the BOTDA detection system

The implementation of the long-range detection system using the BOTDA technique involves three main steps:

- (1) Electronics;
- (2) Electronics, optics and mechanics.
- (3) Software.

5.2.1. BOTDA: Electronics

The development/implementation of the electronic part involves the realization of all the necessary electronic assemblies and sub-assemblies in the composition of the long-range detection system. The major component of this part that must be made is the voltage source that deals with the supply of voltages and currents corresponding to each element that is part of the system:

- the voltage source (the system has a low power consumption, of only ~120W, but one of the sources must be low noise).
- interconnection board (deals with the distribution of voltages and currents to the system elements).
- Auxiliary circuits (ADC 16 bits, ADS1115, and AD8065 for EOM photodetector)
- Data acquisition (AD14-500 from Ultraview, in order to meet the ability to acquire a massive amount of data in the shortest possible time).

5.2.2. BOTDA: Electronics, optics and mechanics

This stage of development covers all elements of the system configuration, including the electronics part, as they cannot be separated very clearly. Practically, to achieve the effective assembly of the long-range detection system, we need all the electronic, optical and mechanical elements. Thus, before starting the assembly process of the long-range detection system, the optical scheme of the system should always be considered. This scheme can be seen in Fig. 5. 4.

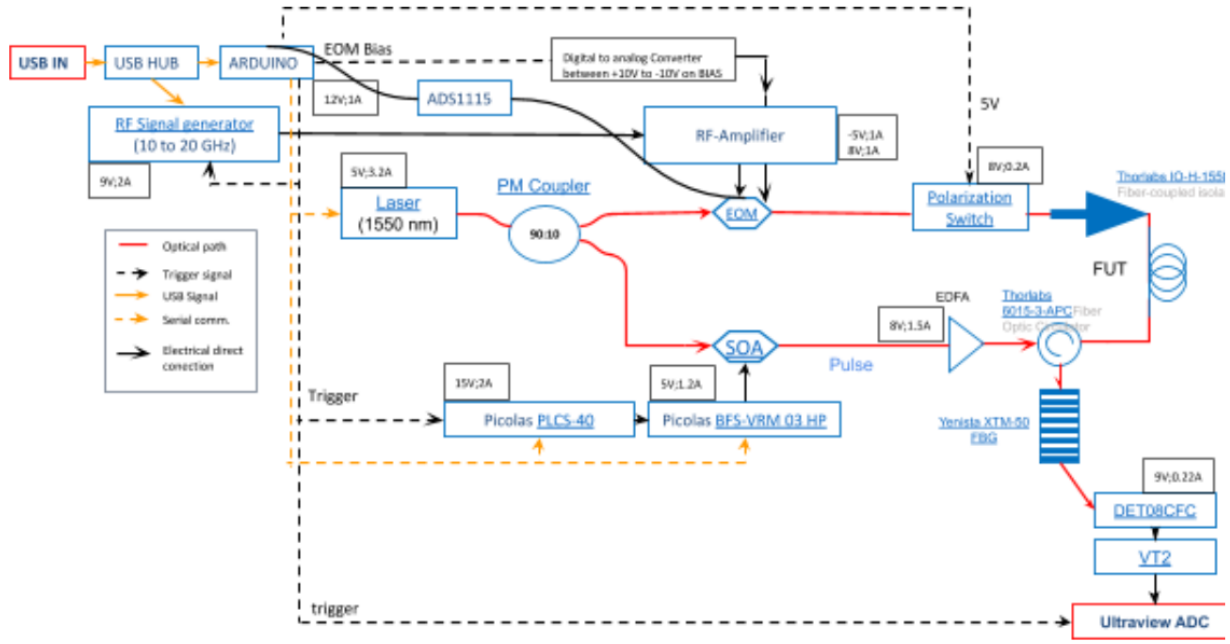

Fig. 5. 4 Electronic and optical scheme of the BOTDA system

Basically, this chapter presents the assembly process of the BOTDA device from the beginning (Fig. 5. 5 on the left side) until the final stage (Fig. 5. 5 on the right side).

Fig. 5. 5 On the left, the first element added to the box, and on the right, the last step..

5.2.3. Software interface for BOTDA

For the long range detection system, 2 software platforms were developed to have a responsive and efficient system. This is also necessary due to the large amount of data generated during an actual acquisition. Thus, there will be a software platform that deals with the data acquisition part and a platform that deals with the data processing part.

5.2.3.1. Software platform – data acquisition

In the image Fig. 5. 6 it is briefly presented the LabVIEW interface for the developed software platform.

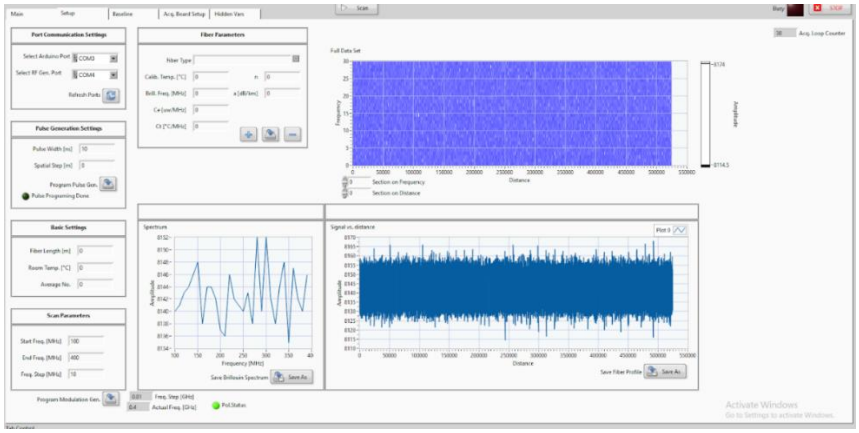

Fig. 5. 6 LabVIEW interface of the software platform

Behind the GUI is a state machine that contains the following options: (1) Init, (2) Init2, (3) Idle, (4) InitScan, (5) FreqandPol, (6) Scan, (7) IniAcq, (8) Acq, (9) Refresh_Graphs, (10) SendPulseConfig, (11) Refresh_Ports, (12) SendModConfig, (13) Exit și (14) Save.

5.2.3.2. Software platform – data processing

The software platform for data processing (Fig. 5. 7) allows uploading 3 sets of data simultaneously to perform their processing. But one of these sets must be the reference set, the rest being experimental data.

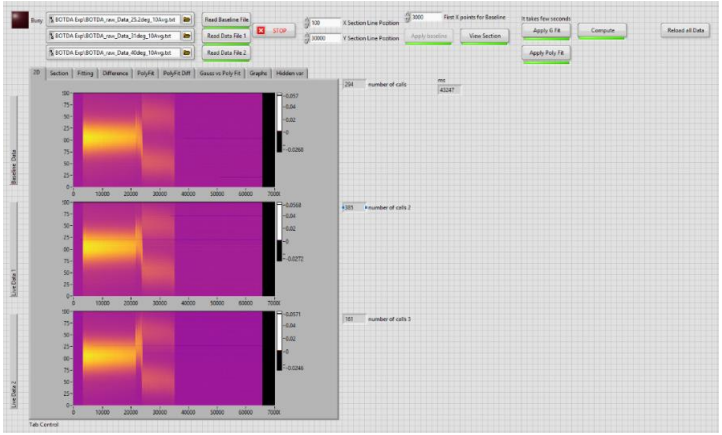

Fig. 5. 7 The new working interface of the LabVIEW program

Thus, an area divided into tabs was created that provides the information according to the operation performed. The program knows how to automatically switch between tabs, depending on the operation performed.

This tabbed implementation of the program done in LabVIEW allows for easier and more compact visualization of the information needed to analyze the data sets. At the same time, the program works more smoothly and easily, because it does not need to refresh all the graphics in the program, but only the ones that are viewed at that moment.

5.2.4. Results obtained with the BOTDA platform

The first datasets generated by this platform were acquired with ZHInst, and the first image was the ramp characteristic of the BOTDA technique for a 50 km optical fiber .

Using the tuned Koheron laser with 100 mA applied along with an optical pulse of 100 ns in length along with connecting a 50 ohm termination, matching attenuation, when the yenista filter was swept the acquisition of data looks like those in the image was presented in Fig. 5. 8.

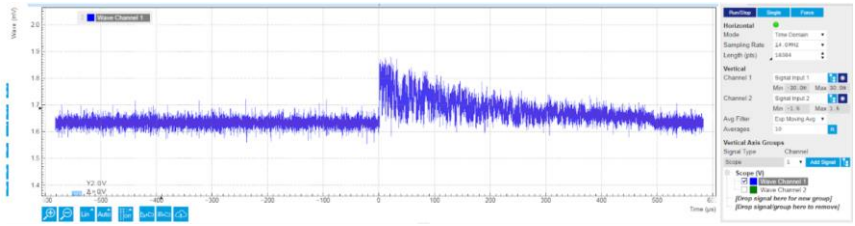

Fig. 5. 8 BOTDA acquired after fine tune-up

Thus, once these results were obtained, thus implicitly the calibration of the system was obtained, a series of experiments could be performed, the simplest and fastest experiment that can be performed being the temperature experiment. Thus, 3 rolls of optical fiber were joined and half of one roll was immersed in a water bath where we have the possibility to increase the temperature in a controlled manner.

In this experiment, 3 sets of data were recorded, one at 25 °C, next at 33 °C and the last one at 45 °C. These data are represented graphically (in the same graph) in the image in Fig. 5. 9.

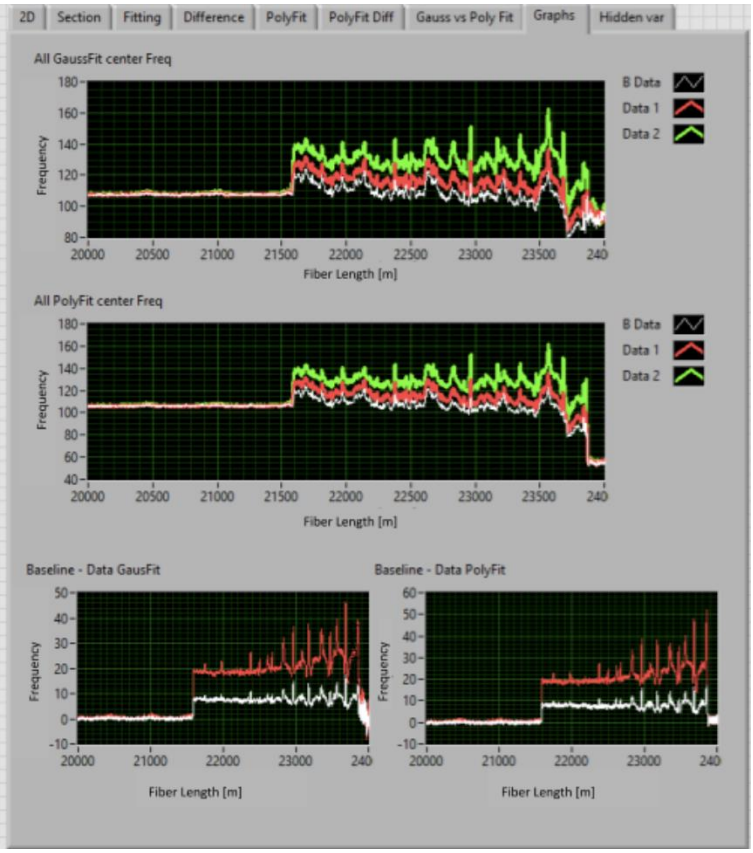

Fig. 5. 9 Screenshot of the LabVIEW user interface comparing Gaussian Fitting and Polynomial Fitting for determining the frequency shifts along optical fiber. The green, red and white curves show the records for a temperature of 25 °C, 33 °C and 45 °C respectively

5. 3. Conclusions

Based on the literature study carried out and presented in Chapter 3, a long distance fiber optic detection system using the BOTDA technique was developed and successfully implemented. Building the system involved identifying, developing, and assembling the components of the electronic, optical, and mechanical parts in its configuration, as detailed in this chapter.

The implementation of the software platforms in LabView for both data acquisition and data processing have also been successfully accomplished and presented descriptively in this chapter.

Tuning of the newly implemented fiber optic long range detection (BOTDA) system was carried out by conducting a series of preliminary experiments. As soon as the system tuning was done, the functionality of the system could be demonstrated by performing experiments to detect temperature variations, using 3 rolls of optical fiber joined together, the intermediate roll being immersed in a water bath, this configuration allowing temperature control.

The proposed higher-order polynomial fitting was shown to achieve over 40 times improvement in computation time compared to a Gaussian fitting method.

In order to demonstrate the performance of the device, the first temperature measurements along the entire length of a 24 km fiber were presented. The measured and processed data shows that the system can quantitatively measure an applied temperature change at a distance of nearly 24 km, thus revealing a frequency uncertainty of ~ 0.2 MHz, which corresponds to a temperature resolution of ~ 0.2 °C and a strain resolution of 4 months. These performances, including the 1m resolution, are maintained for fibers longer than 100km.

5. 4. References

[1] L. Thevenaz, "Brillouin distributed time-domain sensing in optical fibers: state of the art and perspectives," *Frontiers of Optoelectronics in China*, vol. 3, pp. 13-21, 2010.

[2] Corning, "Basic Principles of Fiber Optics, Corning Cable Systems," *[Interactiv]. Available: www.corningcablesystems.com/web/college/fibertutorial.nsf/ofpara.*, 2015 12 Apr..

[3] J. C. J. a. H. F. Taylor, "Distributed fiber optic intrusion sensor system for monitoring long perimeters," *Defense and Security*, pp. 692-703, 2005.

[4] E. Udd, "Fiber optic sensors," 1993.

[5] A. D.-L. A. L.-G. J. A.-C. S. M.-L. a. M. G.-H. X. Angulo-Vinuesa, "Rating the limitations and effectiveness of BOTDA range extension techniques," *International Conference on Optical Fibre Sensors (OFS24*, vol. 4, pp. 96346R-96346R, 2015.

[6] Y. Mao, "Distributed optical fibre sensing system based on Brillouin scattering," *The Hong Kong Polytechnic University*, 2014.

Chapter 6

Realization of a short-range detection system (OFDR technique). Performance in the laboratory with the developed system

6. 1. Introduction

In intrinsic fiber optic sensors using the distributed sensing technique, the optical fiber itself functions as the sensing element. The structure of an optical fiber generally consists of an elongated cylindrical shape, Ge-doped SiO_2 core with a refractive index of about 1.54, embedded in a lower IR glass, covered with protective plastic layers (Fig. 6. 1 a). Fig. 6. 1 b shows how such a simple system can be modeled to work with a distributed sensing mechanism [1, 2, 3].

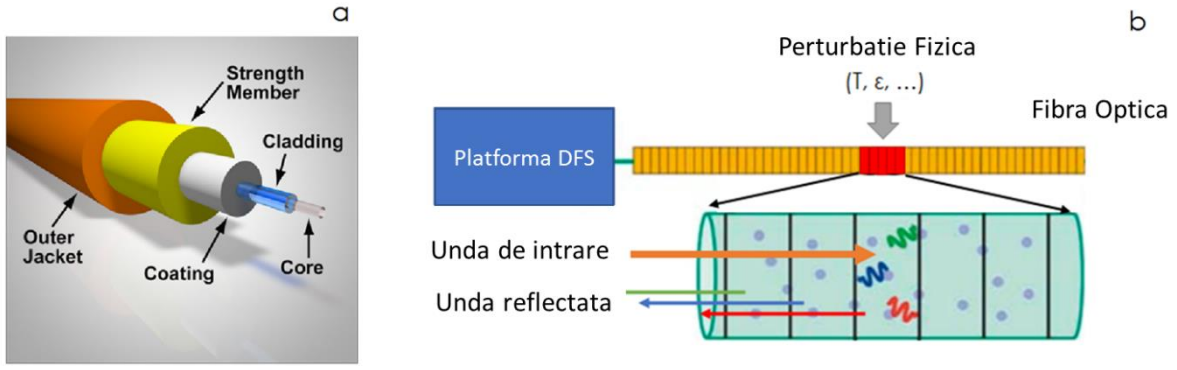

Fig. 6. 1 a). The geometry of an optical fiber, with the outer [4]. b). The working principle of a generic DFS system. A fiber can be modeled as a sequence of adjacent sections. A physical perturbation (e.g. temperature change, strain, acoustic wave, etc.) changes the local state of the fiber, thus resulting in a change in the reflected light wave

When some physical event occurs in one of these imaginary fiber sections, light is scattered in that section with a slightly perturbed frequency, phase, or amplitude. Scattered light is detected by a DFS (Distributed Fiber Sensing) platform, which can individualize the location of the event along the length of the fiber.

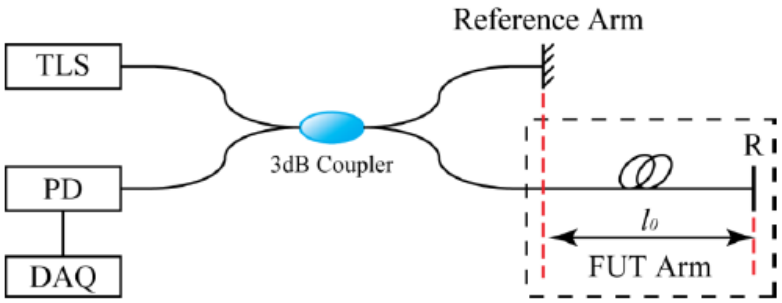

Fig. 6. 2 OFDR system schematic [5]

The key benefits of OFDR technology are the laser-generated quasi-continuous wave modes and the narrowband detection of the optical backscattered signal, which achieves a significantly higher signal to noise ratio compared to conventional pulse technology (OTDR or BOTDA).

The configuration of the OFDR technique requires access to only one of the ends of the optical fiber, as can be seen in the image in Fig. 6. 2**Error! Reference source not found.**. This can be considered an advantage compared to systems that uses BOTDA technique, but the fact that they cannot be used over long distances is a limitation.

6. 2. OFDR Implementation (short range detection)

In order to have an efficient implementation process of the short-range detection system, the realization of the necessary assemblies and sub-assemblies were grouped into three main categories:

- (1) Optics and mechanics;
- (2) Electronics;
- (3) Software.

6.2.1. OFDR: Optics and mechanics [6]

This stage involves the realization and implementation of both the optical and mechanical subassemblies, which are presented together because no clear division can be achieved between them. This optical scheme of the system can be seen in the image from Fig. 6. 3.

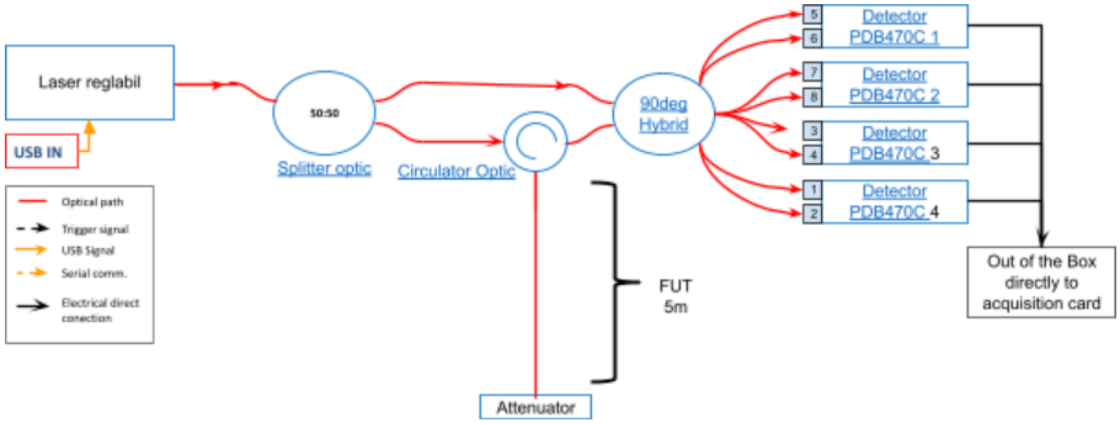

Fig. 6. 3 Optical schematic of the short-range detection system

After going through all the steps in this chapter we get a short range detection platform as shown in the pictures in Fig. 6. 4.

Fig. 6. 4 Final result of the box assembly for the short-range detection platform (front and back view with the cover on)

6.2.2. OFDR: Electronics

From an electronic point of view, the system has a simple configuration consisting of 2 main paths, as follows:

1. The power supplies of the balanced detectors are the original ones, so each one must be connected to 220V. To do this, it was decided to make a block-type assembly and a general panel for the power supply was developed, which was 3D printed.
2. The signals from each balanced photodetector, as we specified in the mechanical assembly, are sent to the NI distribution board and from there with the special NI cable to the NI PCIe 6376 acquisition board.

6.2.3. OFDR Software platform

The system's software interface allows the user full control over the entire platform infrastructure. The program of the short-range detection platform follows the operation diagram shown in Fig. 6. 5.

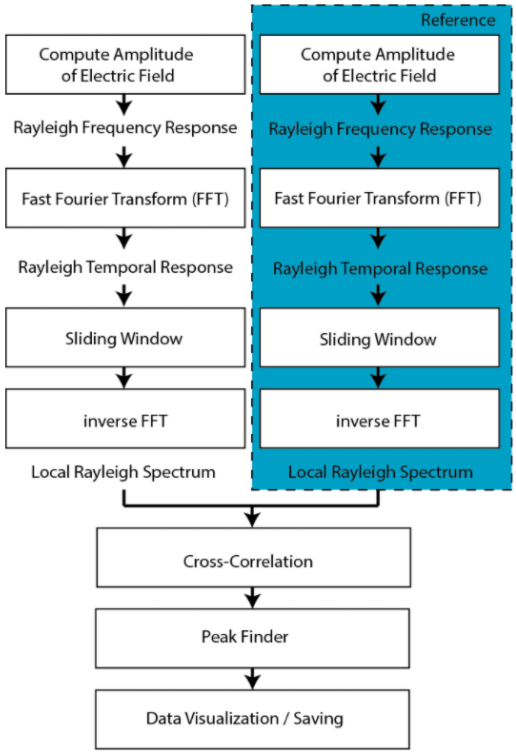

Fig. 6. 5 Flowchart of data processing to extract the Rayleigh frequency shift from the output of the balanced photodetector signals

The resulting software interface is a dynamic one, composed of a series of tabs as can be seen in Fig. 6. 6. This interface allows the user to control all data acquisition parameters coming from the detection platform.

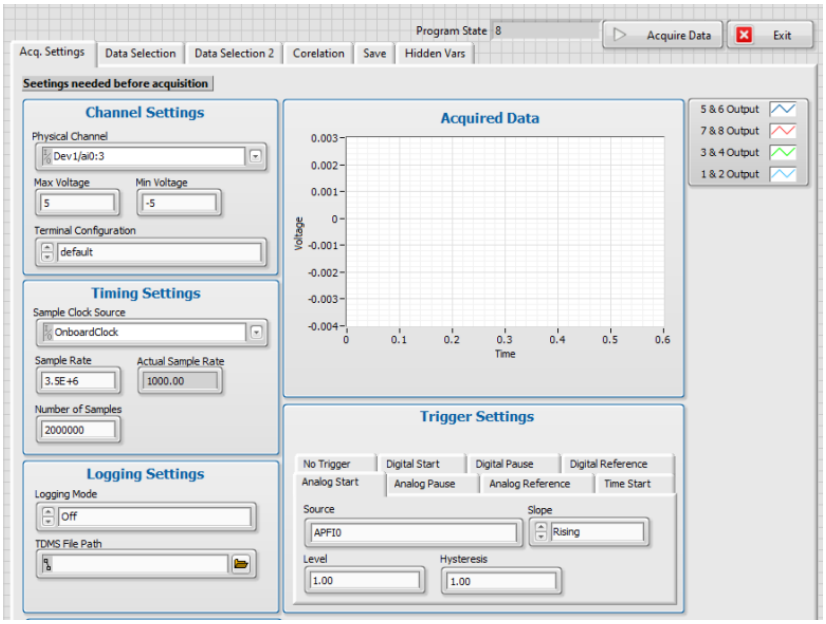

Fig. 6. 6 Acquisition software interface

6. 3. Mass flow Monitoring – experiment [7], [8], [9]

As a result of the process of development and implementation of the short-range detection system, new interesting experimental ideas appeared, which, when implemented, later led to the writing of an article published in a scientific journal [7]. To perform this experiment, both an automated testing system and a small software platform were developed to retrieve and process/analyze the data during the experiment.

The experiment aims at a simple objective, the detection of the flow of a fluid through a tube with the help of an optical fiber mounted inside this tube, being equipped with a heater on the outside (Fig. 6. 7, Fig. 6. 8).

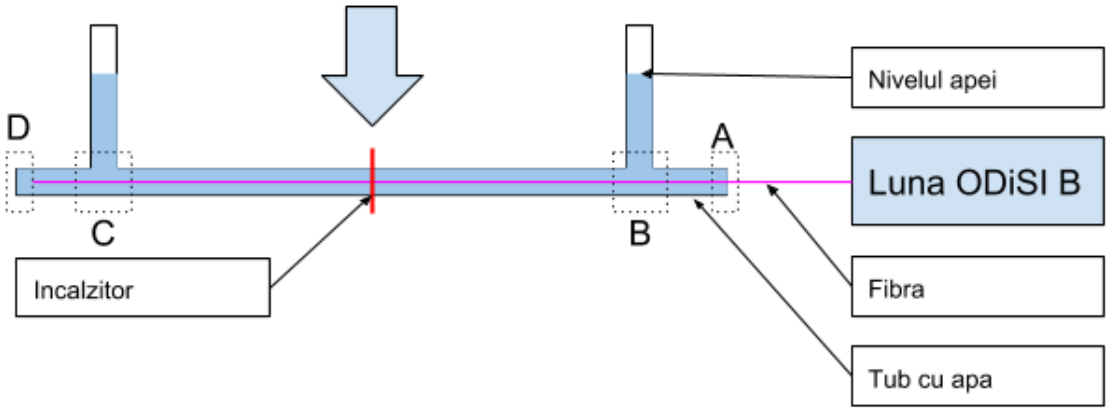

Fig. 6. 7 Configuration and implementation schematic of "fiber flower"

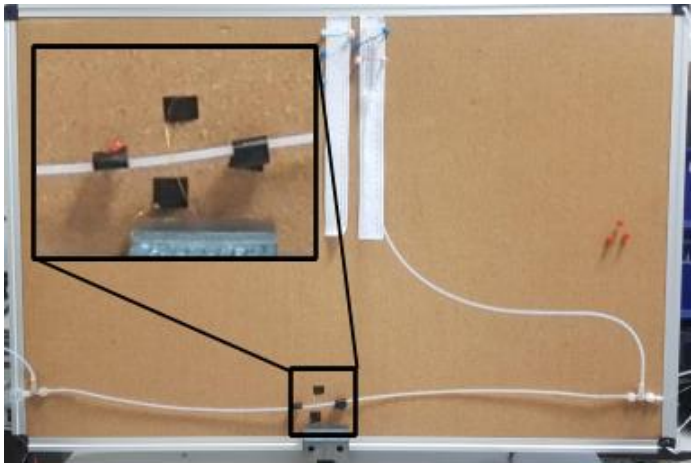

Fig. 6. 8 Real representation of the resulting setup

As it can be seen in Fig. 6. 9, we managed to create a model that faithfully copies the real experiment. We implemented a finite element analysis that solves the fluid dynamics along with the heat transfer equations (these were implemented in Comsol Multiphysics).

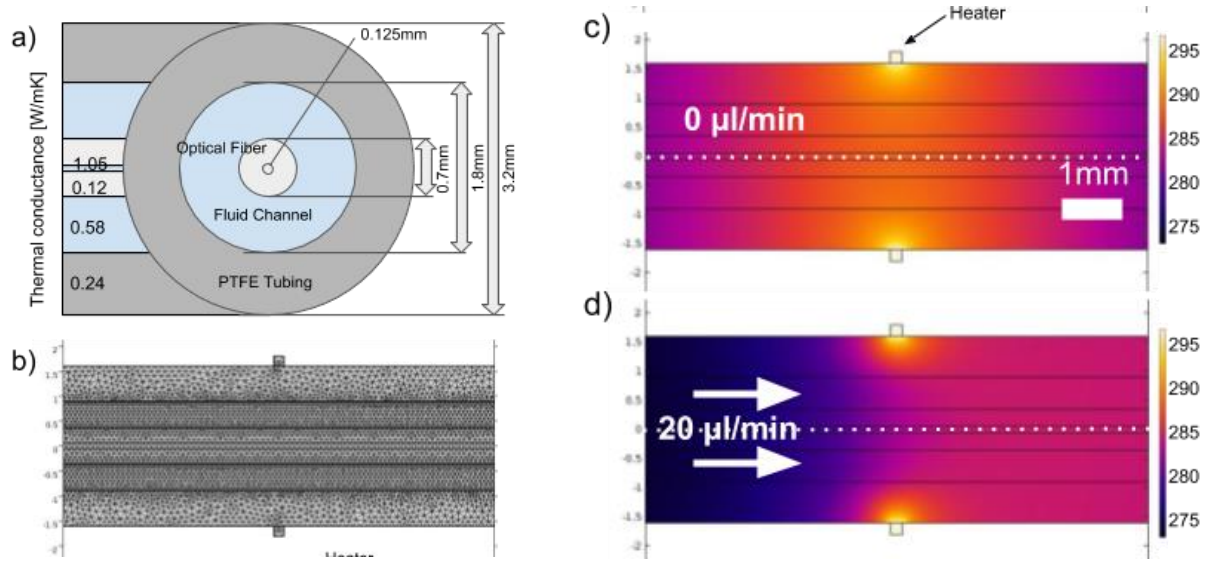

Fig. 6. 9 a) The cross-section of the fluidic tube with integrated optical fiber showing the dimensions and thermal conductivities used for finite element analysis; b) longitudinal cross-section of the model showing the mesh size and the resulting velocity profile; c) the resulting temperature distribution in the absence of flow is symmetrical and centered around the location of the heater; d) In the presence of a flow rate of 20µl/min, heat transport by forced convection changes the downstream temperature profile; The fiber optic temperature profile is taken at the dotted white line as shown

The heat distribution is centered around the heating element for zero flow (Fig. 6. 9 c) and moves downstream with increasing flow velocities and time (t = 235s).

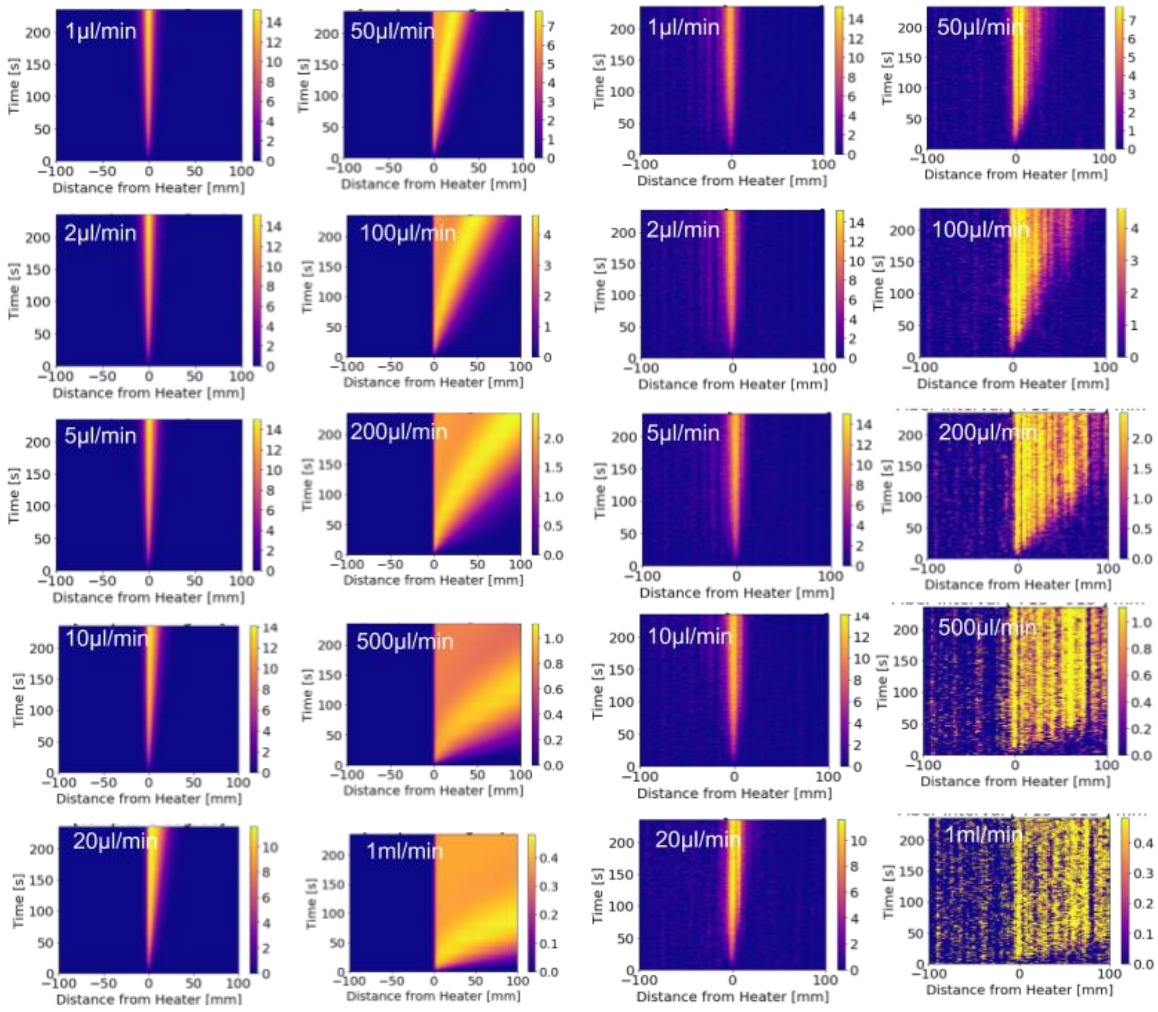

Fig. 6. 10 On the left the finite element analysis and on the right the experimental results regarding the heat distribution for the first 235 seconds after the start of heating and the flow rates vary from 1 µl/min to 1 ml/min.

As can be seen in Fig. 6. 10, the data obtained from the simulation perfectly matches the data sets obtained experimentally. Both images use the same color scale, time intervals and distance, thus allowing us an easy comparison. The experimental result recorded in one dimension along the fiber is consistent with 2D finite element analysis that couples fluid dynamics with heat transfer equations.

6.3.3. Software implementations

In order to accomplish all of the above, a program was developed in LabVIEW. In Fig. 6. 11 the working software interface of the developed program can be seen.

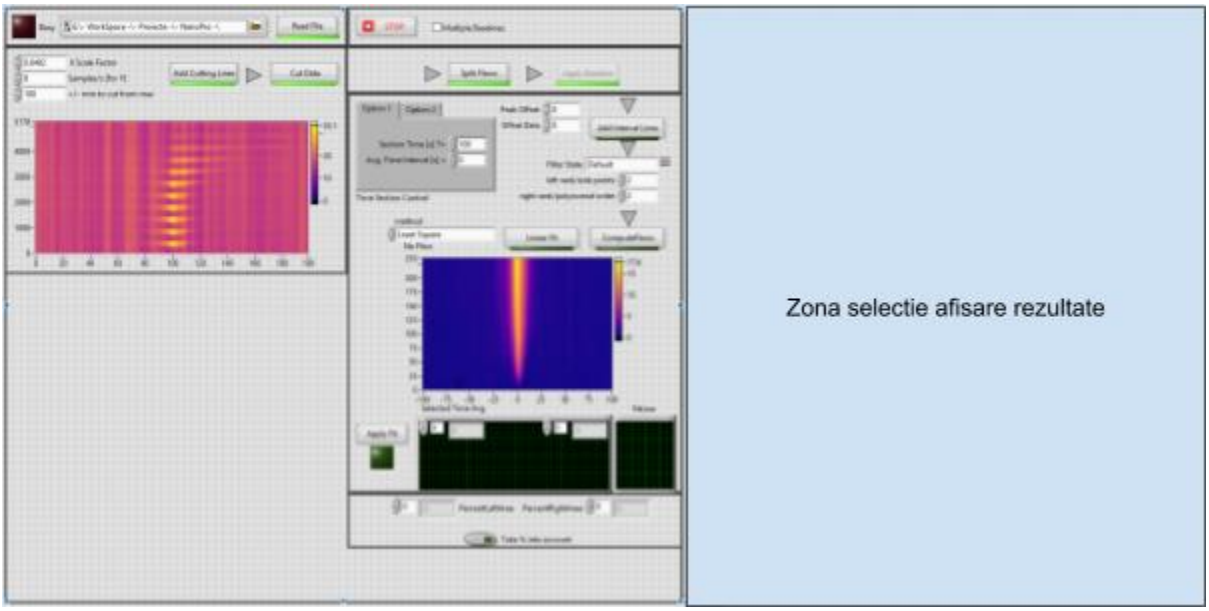

Fig. 6. 11 Image of user interface

As can be seen, the program has a dedicated area that offers the user the possibility to modify the displayed results. That area is divided into tabs, this solution being necessary to allow the viewing of a wide range of information, the display area not being extensive enough for all of them.

6. 4. Conclusions

6.4.1. Conclusions – mass flow monitoring

As presented above, we have discovered a new method of measuring the flow rate in a fluidic pipe by monitoring the heat flow under forced convection. Unlike many other flow measurement techniques, this fiber-optic method has no moving parts, is non-intrusive, and operates under harsh conditions, including high temperatures, high pressures, corrosive environments, and strong electromagnetic environments.

To present the results, I have refined some of the previously presented figures that compares the finite element results with the experimental data. Qualitatively comparing the two

pieces of information we observe a good match between the simulation and the experimental results. We quantified the asymmetry of the temperature distribution with respect to the position of the heater. We summed the superheat temperatures separately for all data points upstream (l) and downstream (r) of the heater location (x = 0 mm).

$$l = \sum_{x=-\infty}^{0} T(x), r = \sum_{x>0}^{\infty} T(x), S = r + l,$$

where *T (x)* are the measured superheat temperatures and S is the sum of all recorded superheat temperatures.

Fig. 6. 12 depicts the upstream (l) temperatures in red, and downstream (r) temperatures in blue versus three orders of magnitude of flow rates. Both simulation (left) and experimental (right) results show data obtained for times t = 50, 100, 150, and 200 s. As flow rates increase, we see an increase in heat moving from upstream to downstream locations. In the simulation, if no heat leaves the system through radiative losses, the heat builds up over time until it is subtracted from the convective flow in the observed element (see flows of 200 µl/min and higher).

In the simulation data, we observe a substantially larger downstream heat build-up than in the experimental data (blue curves). This difference can be explained by the fact that losses to the environment are not taken into account in the simulation. However, experimentally there is a heat loss to the surrounding air, resulting in a lower superheat temperature.

To compensate for the heat losses, we normalize both data sets by dividing l and r by their sum S (as shown in Fig. 6. 12 b). The percentage of heat transferred from the upstream locations to the downstream locations is 50% for zero flow conditions and reaches almost 100% for 1000 µl/min. This measure turns out to be much less independent of the time at which the data points were collected.

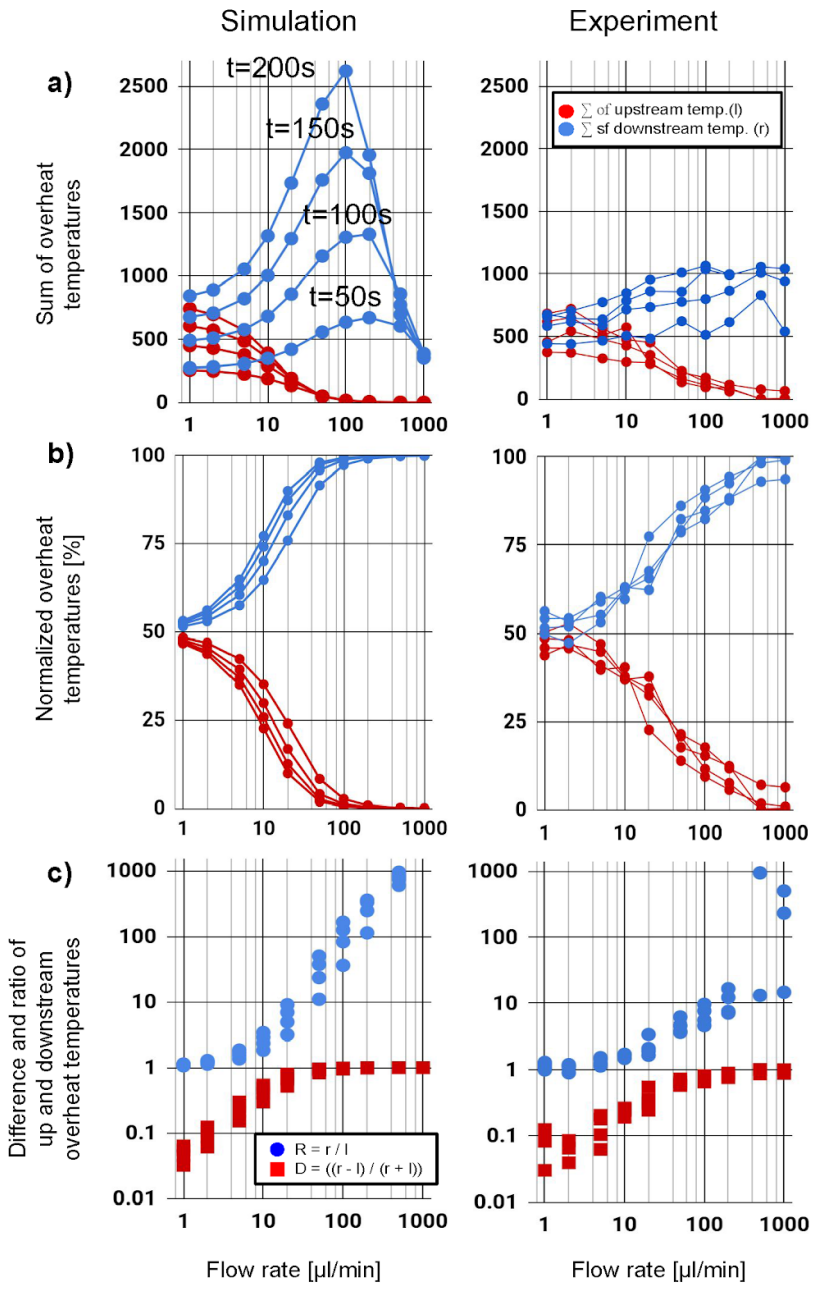

Fig. 6. 12 Comparison of FEA simulation (left) and experimental results (right). a) Superheat temperatures for upstream (red) and downstream (blue) are plotted against flow rate. Data for time t = 50, 100, 150 and 200 s are shown. b) Normal superheat temperatures c) Differential D (red) and ratio R (blue) of upstream and downstream values. While for low flow rates (<10 µl/min) the difference presents a more favorable metric, the ratio (R in blue) presents a better response for high flow rates (>10 µl/min)

We introduced into the study a temperature difference (D) between upstream and downstream given by D = (r-l)/s (red squares in Fig. 6. 12 c). D is independent of superheat temperature and increases monotonically with flow rate. For flow rates above 10 µl/min, the differential signal asymptotically approaches 1. This is because in a convection-dominated regime it no longer diffuses heat upstream and l approaches zero. D reaches 1 for the no-flow condition where only diffusion contributes to the heat flux and r = l.

A second metric is the ratio (R) of l and r, R = (r / l) -1. (Blue dots in Fig. 6. 12 c). R is 1 for zero flow rates and increases monotonically with flow rates. While for low flow regimes (<10 µl/min) in the diffusion-dominated regime the difference (D) is a favorable metric, the ratio (R) shows a better response for high flow rates (> 10 µl/min) where it dominates convection. Except for a few data points for a very low flow rate of 1 µl/min and very high flow rates, both curves show a monotonic increase with flow rates and can therefore be used for detection. Based on these results, the lower detection limits are less than or equal to 2µl/min (more precisely 32nl/min). A detailed analysis of the upper and lower detection limits of the system is part of planned future work. These detection limits are related to the lateral and thermal resolution of the fiber optic temperature detection method. Low detection limit combined with high dynamic range outperforms many other flow detection techniques.

6.4.2. Conclusions – OFDR platform

Tests were also carried out with the temperature in the water bath.

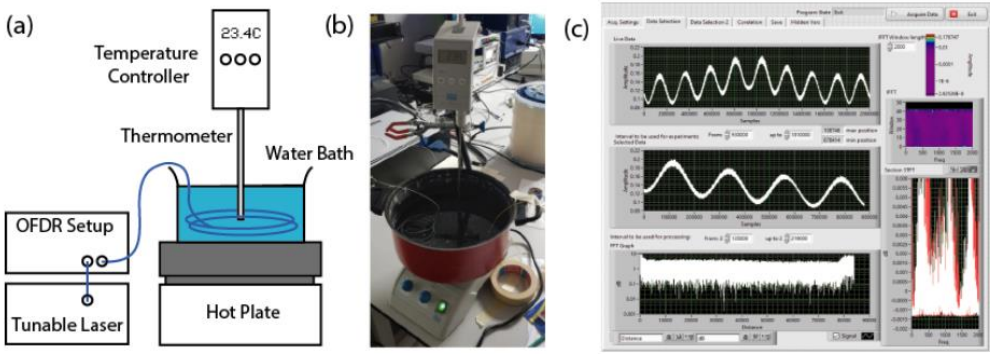

Fig. 6. 13 Experimental setup for temperature sensing (a) Schematic and (b) photograph of the simple experimental setup for temperature sensing. c) software platform for temperature monitoring

While the water temperature is increased, the data measured by the OFDR setup is recorded using the interface developed in LabVIEW. Using the measurement at 25 °C as a reference, the resulting correlation maps for 12 different temperatures ranges from 25 °C to 37 °C. As expected, a clear correlation peak results where the fiber has not been heated, for example at a distance of 150 cm, the correlation of the measured Rayleigh spectrum with itself at temp. of 25 °C. Where the fiber is submerged in water (approximately from 25 cm to 100 cm) the temperature increases and the Rayleigh frequency gain of the submerged section of optical fiber also increases.

The results show that for small temperature changes of up to a few degrees Celsius relative to the reference, we can see a clear detection of the peak location, resulting in a reliable measured temperature profile (see e.g. 30 and 35 °C); however, in general for larger temperature changes the peak detection and recovered temperature profile becomes less accurate.

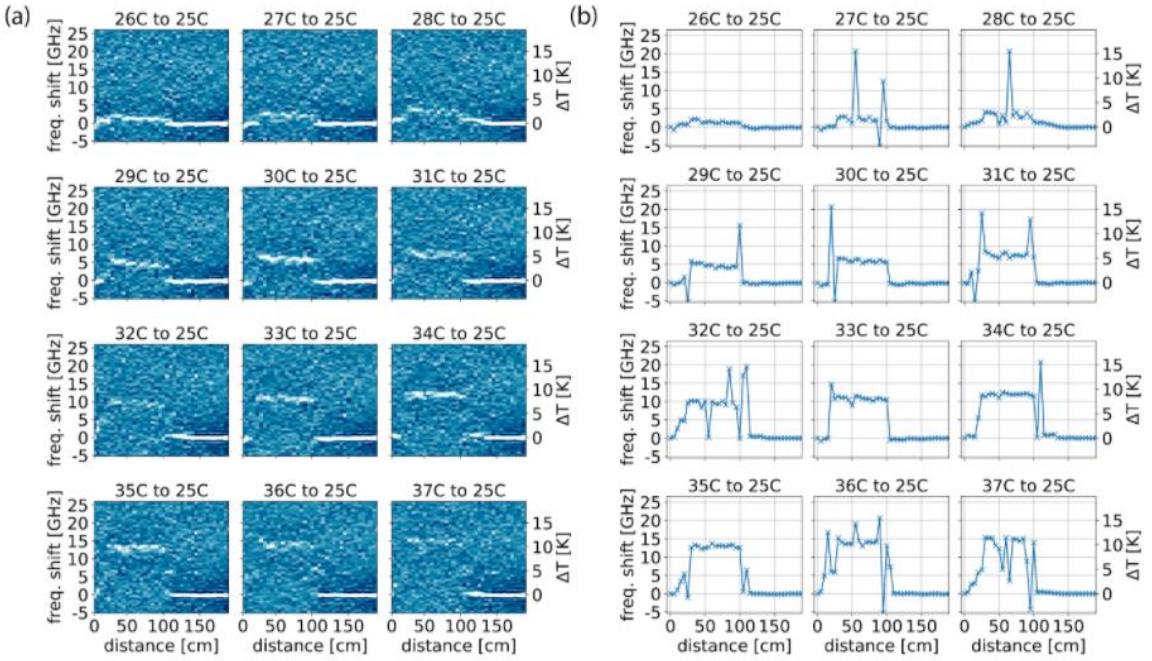

Fig. 6. 14 (a) Distributed differential correlation maps retrieved for 12 temperatures between 25°C and 37°C. (b) Retrieved temperature profiles show that detection of the correlation peak becomes unreliable with larger temperature differences as the correlation amplitude decays

In order to measure large temperature changes, or equivalently large stress variations, the correlation peak can be obtained by updating the reference traces when the correlation peak moves

more than a given threshold value. Updating the reference every time the correlation frequency change varies by more than 1.2 GHz (roughly corresponding to the temperature change of about 1K), the differential temperature maps for the 12 temperatures shown previously are recalculated and shown in Fig. 6. 15 a, while Fig. 6. 15 b illustrates the resulting differential temperature profiles. The results demonstrate a more reliable extraction of the temperature profile compared to the case reported in Fig. 6. 14.

Knowing the reference temperature profile and tracking the Rayleigh frequency shift for each of the reference updates, the distributed absolute temperature profile can be obtained as reported in Fig. 6. 16 a. The temperature resolution is obtained by the standard deviation of the temperature profile at the fiber location that is not affected by temperature changes, thus resulting in a resolution of 0.1 K and for stress a resolution below με; while the spatial resolution is 5 cm, being in this case limited by the spatial sampling rate.

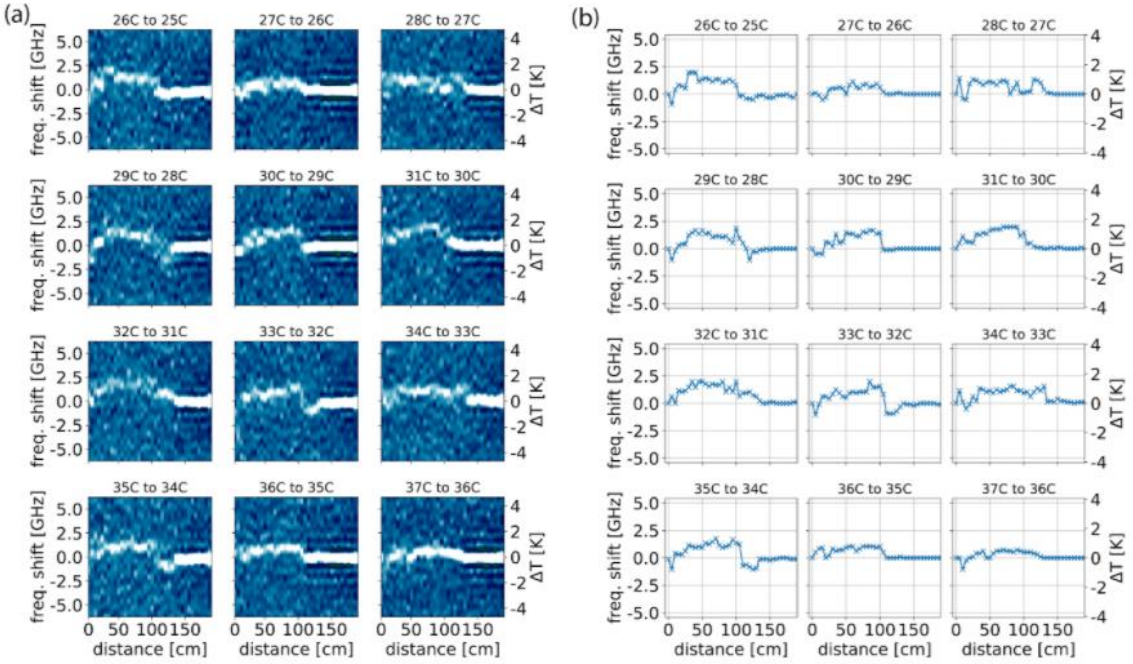

Fig. 6. 15 (a) Distributed maps of differential temperature for 12 temperatures between 25°C and 36°C, when correlating each data set with the previous one. (b) Retrieved differential temperature profiles

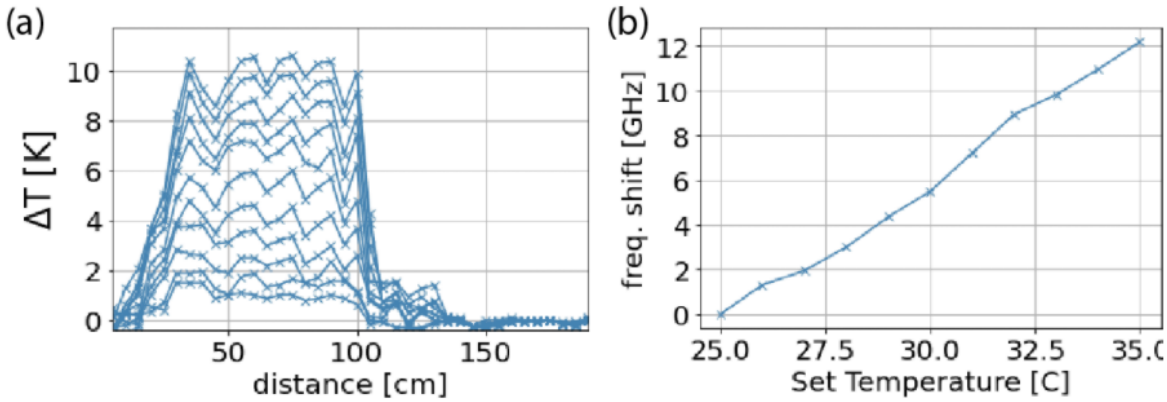

Fig. 6. 16 (a) The distributed temperature profile along the sensing fiber obtained by continuously updating the reference traces. (b) scatterplot of frequency change versus temperatures recorded with a thermometer. We observe a linear response with a sensitivity of 1.2 GHz / K

In Fig. 6. 16 b we show the average of the frequency changes found at 40 cm and 80 cm, where the fiber was completely submerged in water. Frequency changes are displayed based on temperatures actually measured using an accurate thermometer. The result shows good linearity, from the linear fitting we observe a sensitivity of 1.2 GHz/K, which is expected and typical for silica-based optical fibers.

6. 5. Refences

[1] L. Thevenaz, "Brillouin distributed time-domain sensing in optical fibers: state of the art and perspectives," *Frontiers of Optoelectronics in China,* vol. 3, pp. 13-21, 2010.

[2] Corning, "Basic Principles of Fiber Optics, Corning Cable Systems," *[Interactiv]. Available: www.corningcablesystems.com/web/college/fibertutorial.nsf/ofpara.*, 2015 12 Apr..

[3] J. C. J. a. H. F. Taylor, "Distributed fiber optic intrusion sensor system for monitoring long perimeters," *Defense and Security,* pp. 692-703, 2005.

[4] M. W. V. M. P. M. Kivilcim Yuksel, "Optical frequency domain reflectometry: A review," in *11th International Conference on Transparent Optical Networks*, Ponta Delgada, Portugal, 2009.

[5] J. Song, "Optical Frequency Domain Reflectometry: Sensing Range Extension and Enhanced Temperature Sensitivity.," *Université d'Ottawa/University of Ottawa,* 2014.

[6] M. A. S. M. E. D. Z. Jderu Alin, "Realization of a polarization-insensitive optical frequency-domain reflectometer using an I/Q homodyne detection," vol. Journal of the European Optical Society Rapid Publications , 2021, DOI:10.1186/s41476-021-00165-8.

[7] M. E. D. Z. Alin Jderu, "Mass Flow Monitoring by Distributed Fiber Optical Temperature Sensing," *Sensors, DOI:10.3390/s19194151,* 2019.

[8] M. A. S. M. E. D. Z. Jderu Alin, "Liquid Flow Meter by Fiber-Optic Sensing of Heat Propagation," *Sensors,* 2021, DOI:10.3390/s21020355.

[9] D. Z. M. E. Jderu Alin, "Metoda si dispozitiv pentru monitorizarea calorimetrica a debitului sau fluxului de fluid or masa". Romania 2018.

Chapter 7

General conclusions

7. 1. Atomic force microscope

In this PhD thesis, a detailed study on the performance of AFM techniques and systems currently available on the market was successfully carried out. The study led to the finalization of the design and development of an atomic force microscope with multiple elements of originality (measurement head with a new design, new electronic modules, new software platform, etc.) capable of working both in contact mode at atomic resolution and also in non-contact mode with a vertical resolution of 0.01 nm, capable of imaging small areas, but also extended areas (up to approximately 50x50 μm^2), in multiple environments (ambient conditions, in an environment with controlled humidity, in an environment of inert gases or in vacuum up to 10^{-4} torr).

The technique and the resulting system has been experimentally tested with special calibration samples for such devices, such as the TGZ02 grid that has a z-step of 110nm, and the results are very good, as can be seen in Fig. 7. 1.

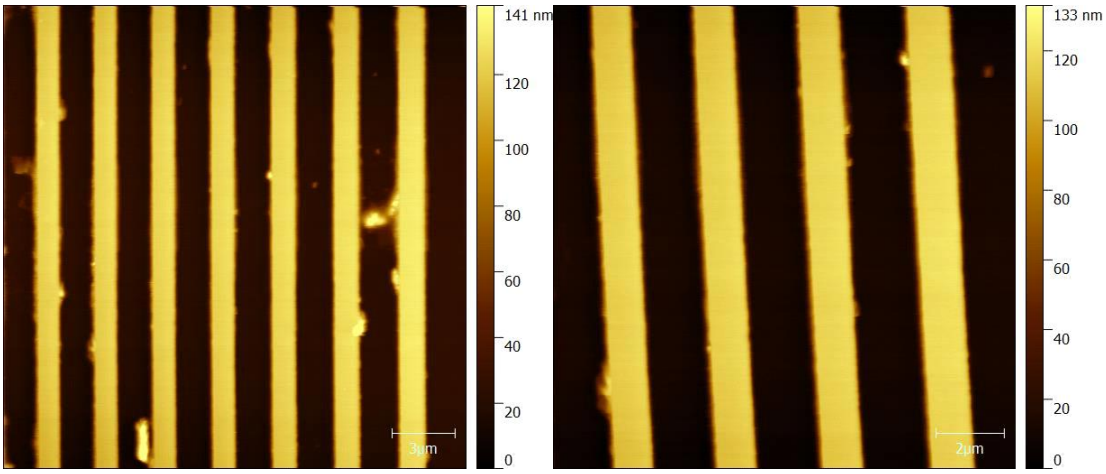

Fig. 7. 1 Topography image for the TGZ02 calibration grid; On the left is the profile obtained on a large area and on the right is a scan on a restricted area.

The real performance of the system is highlighted in Fig. 7. *2* where the achievement of atomic resolution under ambient conditions (room temperature, humidity RH 55%) is demonstrated on a freshly cleaved mica sample.

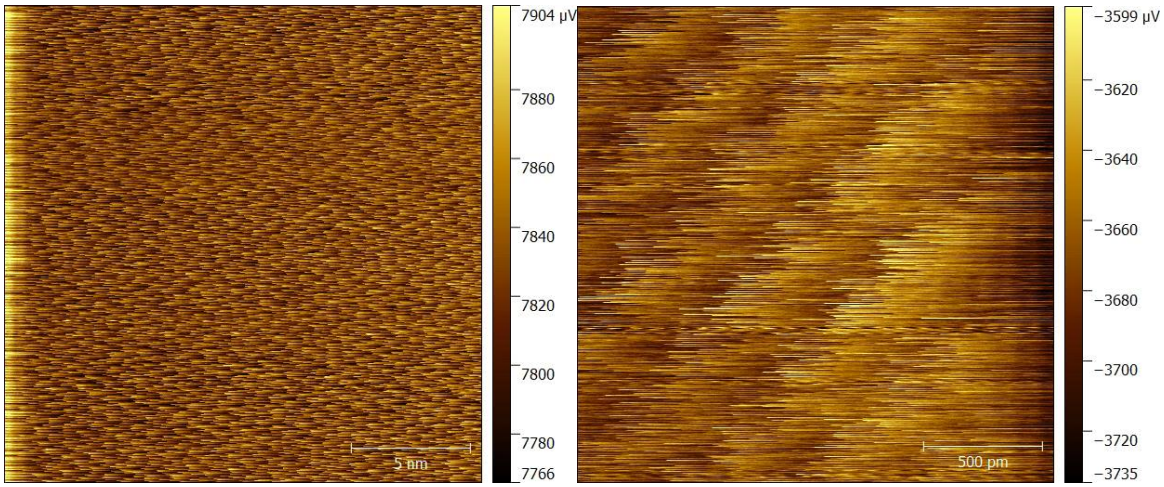

Fig. 7. 2 *Atomic resolution achieved with the constructed microscope.*

The fact that the constructed AFM system is capable of atomic resolution imaging demonstrates its ability to achieve the highest resolutions in all common AFM modes, such as AFM topography, AFM-conductive, etc.

7. 2. BOTDA

In order to understand as precisely as possible the working principles of long range fiber optic detection techniques, as well as the progress made by researchers and engineers in this development and optimization, a research study was carried out that set the starting point for the system of long range detection.

The performance of the system has been demonstrated since the first temperature measurements along the entire length of a 24 km fiber. The measured and processed data shows that the system can quantitatively measure an applied temperature change at a distance of nearly 24 km, thus revealing a frequency uncertainty of ~ 0.2 MHz, which corresponds to a temperature resolution of ~ 0.2 °C and a strain resolution of 4 με.

As it can be seen, based on the results obtained and the performance of the BOTDA technique, the system can thus detect changes of 0.2 °C or 4 με over a distance of more than 100 km with a spatial resolution of 1 m.

Such a device has an important applicability in many fields of activity such as: oil industry, monitoring of buildings, lakes, in drilling industries, as well as intrusion detection (due to the high sensitivity of the fiber it is possible to differentiate between the vibrations produced by a human or by a car, for example).

In Fig. 7. 3 it can be seen how an optical fiber, consisting of 3 fiber coils, presents 3 different temperature zones. The boxed area in this image corresponds to the fiber spool placed in warm water.

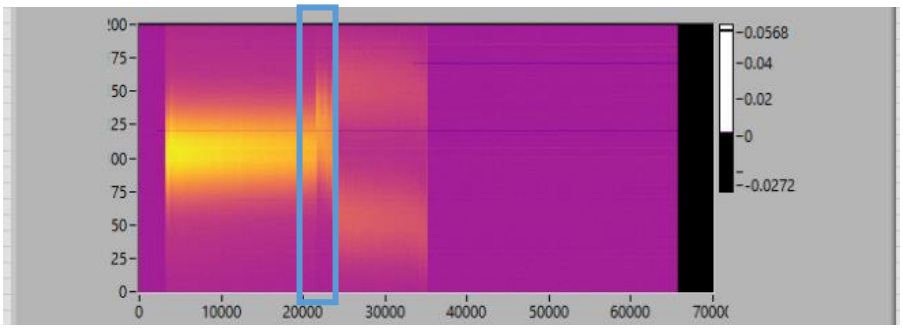

Fig. 7. 3 Image with 3 spools of optical fiber.

At the same time, it was also demonstrated that the proposed higher-order polynomial fitting achieves a more than 40-fold improvement in calculation time compared to a Gaussian fitting method.

7. 3. OFDR

The research study carried out for short-range detection techniques and systems, in terms of their operating principles but also the progress made at the present time set the starting point for the short range detection system.

The results obtained with the OFDR platform Fig. 7. 4 shows that for small temperature changes of up to a few degrees Celsius relative to the reference, we can see a clear detection of the peak location, resulting in a reliable measured temperature profile (see e.g. 30 and 35 °C); however, in general for larger temperature changes the peak detection and recovered temperature profile becomes less accurate.

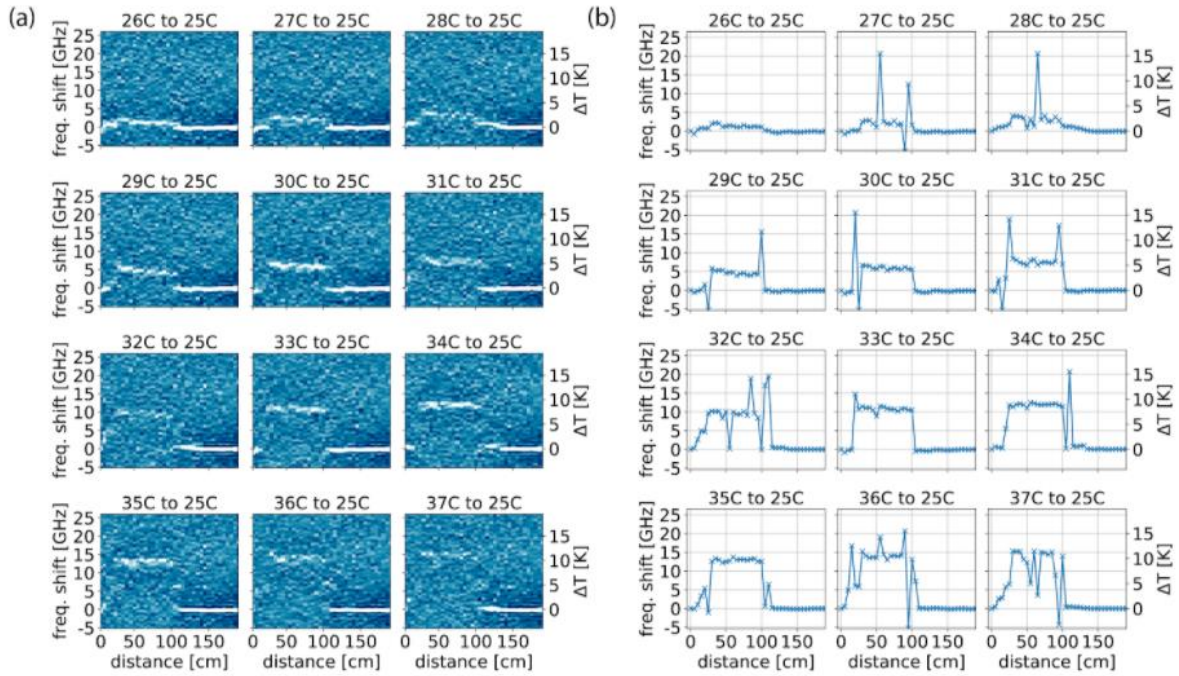

Fig. 7. 4 (a) Distributed differential correlation maps retrieved for 12 temperatures between 25℃ and 37℃. (b) Retrieved temperature profiles shows that detection of the correlation peak becomes unreliable with larger temperature differences as the correlation amplitude decays

To measure large temperature changes, or equivalently large stress variations, the correlation peak can be obtained by updating the reference traces when the correlation peak moves more than a given threshold value. Updating the reference every time the correlation frequency change varies by more than 1.2 GHz (roughly corresponding to the temperature change of about 1K), the differential temperature maps shown previously are recalculated and shown in Fig. 7. 5.

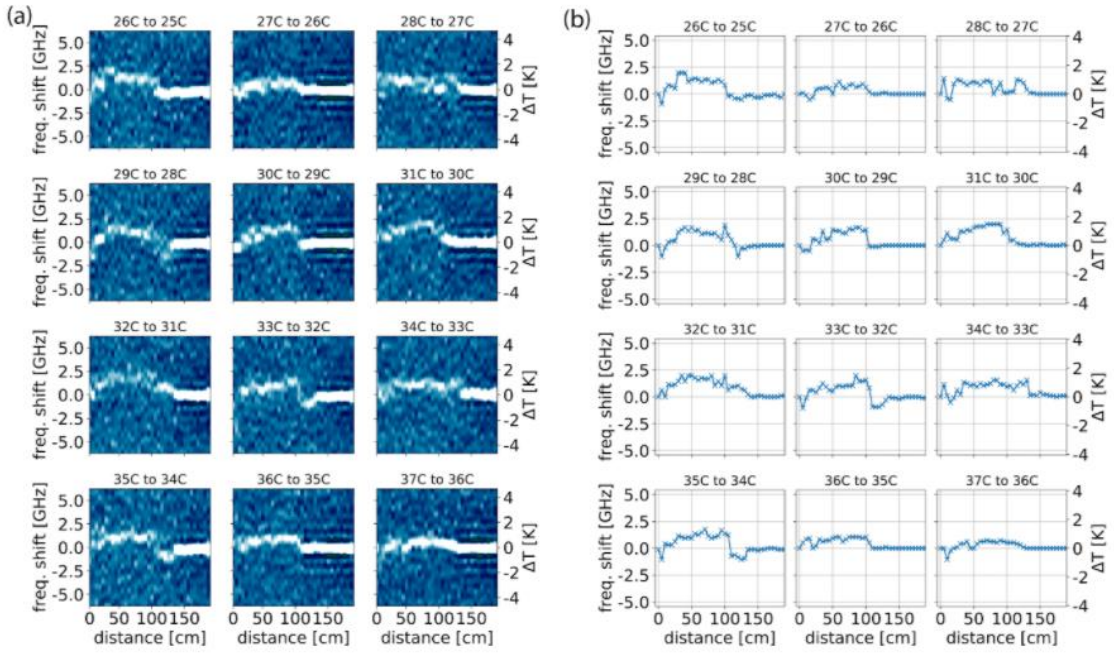

Fig. 7. 5 (a) Distributed maps of differential temperature for 12 temperatures between 25°C and 36°C, when correlating each data set with the previous one. (b) Retrieved differential temperature profiles

As it can be seen, based on the obtained results and the performances of the OFDR technique, the system can thus detect changes in the order of °C or deformation in the order of με over a distance of several meters with a sub-micrometric resolution.

Such a device has an important applicability in many fields of activity such as: the medical industry, the beverage and food industry, the semiconductor industry, dirty water monitoring but also for measuring the flow rates of dangerous or highly corrosive substances.

7. 4. Mass Flow Monitoring

As I presented in this PhD thesis, I discovered a new method for measuring the flow rate in a fluidic pipe by monitoring the heat flow under forced convection. Unlike many other flow measurement techniques, this fiber-optic method has no moving parts, is non-intrusive, and operates under harsh conditions, including high temperatures, high pressures, corrosive environments, and strong electromagnetic environments.

Fig. 7. 6 depicts upstream (l) temperatures in red, and downstream (r) temperatures in blue versus three orders of magnitude of flow rates. Both simulation (left) and experimental

(right) results show data obtained for times t = 50, 100, 150, and 200 s. As flow rates increase, we see an increase in heat moving from upstream to downstream locations. In the simulation, if no heat leaves the system through radiative losses, the heat accumulates over time until it is subtracted from the convective flow in the observed element (see flow rates of 200 µl/min and higher .

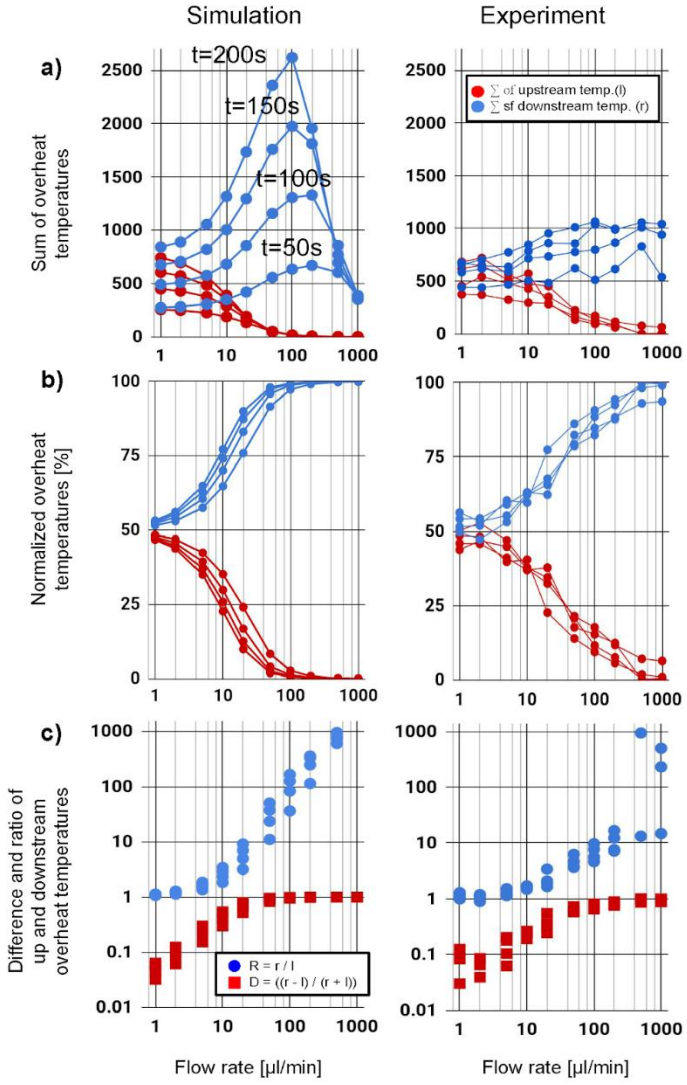

Fig. 7. 6 Comparison of FEA simulation (left) and experimental results (right). a) Superheat temperatures for upstream (red) and downstream (blue) are plotted against flow rate. Data for time t = 50, 100, 150 and 200 s are shown. b) Normal superheat temperatures c) Differential D (red) and ratio R (blue) of upstream and downstream values. While for low flow rates (<10 µl/min) the difference presents a more favorable metric, the ratio (R in blue) presents a better response for high flow rates (>10 µl/min)

In the simulation data, we observe a substantially larger downstream heat build-up than in the experimental data (blue curves). This difference can be explained by the fact that losses to the environment are not taken into account in the simulation. However, experimentally there is heat loss to the surrounding air, resulting in a lower superheat temperature.

To compensate for heat losses, we normalize both data sets by dividing l and r by their sum S (as shown in Fig. 6. 51 b). The percentage of heat transferred from the upstream locations to the downstream locations is 50% for zero flow conditions and reaches almost 100% for 1000 µl/min. This measure turns out to be much less independent of the time at which the data points were collected.

As it can be seen, based on the results obtained and the performances of the OFDR technique implemented in this flow measurement method, the system can thus measure flow rates from 32 nl/min to 1000 µl/min without requiring modifications or reconfiguration.

Such a device has an important applicability in sensitive fields of activity such as: the medical industry for the delivery of extremely precise medicines, but also for measuring the flow rates of dangerous or extremely corrosive substances

7. 5. Future perspectives

The results presented in this thesis present the successful implementation of an atomic force microscope for large and small surfaces, as well as two platforms for detecting temperature and stress over long and short distances, respectively.

Although the techniques and devices are complete and perfectly functional at this point, there is still room for evolution and improvement. For example, for the AFM system, special software modules can be developed for specific scanning techniques, such as sample conductivity mapping.

As for long-range detection systems, pattern recognition modules can be developed for them and thus, using the ability of fibers to sense stress, clear differences can be made between vibrations made by a human, machine or other sources. Thus the system can be successfully used for intrusion detection using a single sensor.

Short-range systems, on the other hand, benefit from the very high precision and resistance of optical fibers, so they can be successfully used to make extremely precise medical syringes or to monitor flows in radioactive or acid contaminated areas.

As can be seen, the possibilities of evolution from this point are extremely large and extended in many areas.

Scientific Activities

The results of the research obtained in this doctoral thesis have been materialized in the following publications, conferences and patents:

Published Articles:

1. M. A. Soto, **A. Jderu**, D. Dorobantu, M. Enachescu, D. Ziegler and S. Sedighi - „*Swelling-Based Distributed Chemical Sensing with Standard Acrylate Coated Optical Fibers*", Sensors, 2021, DOI:10.3390/s21030718.
2. **A. Jderu,** D. Dorobantu, M. Enachescu, D. Ziegler, M. A. Soto - „*High-Order Polynomial Fitting Assistance for Fast Double-Peak Finding in Brillouin-Distributed Sensing*", Sensors, vol. 21, 2020, https://doi.org/10.3390/s21010187.
3. C. C. Moise, A. Pantazi, G. V. Mihai, **A. Jderu**, M. Bercu, A. A. Messina, M. Enachescu - „*Surface Topography of Si/TiO2 Stacked Layers on Silicon Substrate Deposited by KrF Excimer Laser Ablation*", COATINGS, 11(11), 2021.
4. M. A. Soto, M. Enachescu, D. Ziegler, **A. Jder**u - „*Realization of a polarization-insensitive optical frequency-domain reflectometer using an I/Q homodyne detection*", vol. Journal of the European Optical Society Rapid Publications , 2021, DOI:10.1186/s41476-021-00165-8.
5. M. A. Soto, M. Enachescu, D. Ziegler, **A. Jderu** - „*Liquid Flow Meter by Fiber-Optic Sensing of Heat Propagation*", Sensors, 2021, DOI:10.3390/s21020355.
6. D. Dorobantu, D. Ziegler, M. Enachescu, **A. Jderu** - „*Swelling-Based Chemical Sensing With Unmodified Optical Fibers*", Photonic Sensors, 2021, DOI:10.1007/s13320-021-0637-2.
7. **A. Jderu,** M. Enachescu, D. Ziegler, D. Dorobantu - „*Fabrication of Optical Fibers with Multiple Coatings for Swelling-Based Chemical Sensing*", Micromachines, 2021, DOI:10.3390/mi12080941.
8. M. Enachescu, D. Ziegler, **A. Jderu** - „*Mass Flow Monitoring by Distributed Fiber Optical Temperature Sensing*", Sensors, DOI:10.3390/s19194151, 2019.

9. **A. Jderu**, D. Dorobantu, M. A. Soto, M. Enachescu, D. Ziegler - „*Brillouin Optical Time-Domain Analyzer engineered implementation using high-order polynomial spectral fitting*" – U.P.B. Sci. Bull., Series C, Vol. 85, Iss. 2, 2023 ISSN 2286-3540
10. J. Al-Zanganawee, S. Iftimie, A. Pantazi, R. Mesterca, **A. Jderu,** S. Antohe and M. Enachescu - „*On the physical properties of inverted photovoltaic structures based on P3OT:F-SWCNTs active layer*", Journal of Ovonic Research, vol. 14, no. 4, pp. 287-292, 2018.
11. J. C. Grigore, **A. Jderu**, M. Enachescu - "*Vibrations And Equilibrium Motion Of The Planar Kinematic Chains With And Without Clearance In Joints*", Ciencia e Tecnica Vitivinicola' Journal (ISSN: 0254-0223), Vol. 31, no 6, 0.425., 2016
12. J. C. Grigore, **A. Jderu**, M. Enachescu - "*Vibrations Of A Planar Kinematic Chains Formed By Straight Bars With Rotational Kinematical Links With Clearances*", Ciencia e Tecnica Vitivinicola' Journal (ISSN: 0254-0223), Vol. 31, no 6, 0.425., 2016,
13. A. Barra, N. M. Ferreira, M. A. Martins, O. Lazar, A. Pantazi, **A. Jderu**, S. M. Neumayer, B. J. Rodriguez, M. Enachescu, P. Ferreira, C. Nunes, - „*Eco-friendly preparation of electrically conductive chitosan - reduced graphene oxide flexible bionanocomposites for food packaging and biological applications*", COMPOSITES SCIENCE AND TECHNOLOGY, 173, pag. 53-60, 2019.
14. O. V. Iaseniuc, M. S. Iovu, A. Ghiulnare, R. Mesterca, **A. Jderu**, M. Enachescu, - „*Micro-raman spectra of bulk GexAsxSe1-2x chalcogenide glasses*", PROCEEDINGS OF THE ROMANIAN ACADEMY SERIES A-MATHEMATICS PHYSICS TECHNICAL SCIENCES INFORMATION SCIENCE, 19(4), pag. 545-550, 2018.
15. O. V. Iaseniuc, M. S. Iovu, A. Ghiulnare, R. Mesterca, **A. Jderu**, M. Enachescu - „*Micro-Raman spectra of the amorphous GexAsxSe1-2x chalcogenide glasses*", ADVANCED TOPICS IN OPTOELECTRONICS, MICROELECTRONICS, AND NANOTECHNOLOGIES IX, 10977, 2018.

Scientific Conferences:

1. Aida Pantazi, Oana Brincoveanu, Antoniu Moldovan, **Alexandru-Alin Jderu**, Doru Dinescu, Marius Enachescu - „*Atomic resolution using a home-built atomic force microscope*", Seminarul Național de nanoștiință si nanotehnologie, 2014, București, Romania

2. I. Popa, **A. Jderu,** C. Livede, D. Dorobantu, M. Enachescu - „*Distributed Brillouin Sensors for Simultaneous Temperature and Strain Sensing*", Conference: ARA 40th Congress, The 40th ARA Proceeding, American Romanian Academy of Arts and Science, 2016, DOI:10.14510/40ARA2016.4015.
3. J. C. Grigore, **A. Jderu**, M. Enachescu - „*Application to the Motion and Equilibrium of the Planar Kinematic Chains with Rotational Linkswith Clearances*", Conference: ARA 40th Congress, The 40th ARA Proceeding, American Romanian Academy of Arts and Science, 2016, ISBN: 978-1-4244-4715-2;
4. I. Popa, C. Livede, **A. Jderu**, M. Enachescu - „*A Digital Charge Amplifier Model for Hysteresis Reducing of Piezoelectric Actuators*", Conference: the 39th American Romanian Academy of Arts and Sciences Congress, 2015. . ISBN: 978-1-4244-4715-2;
5. J. C. Grigore, **A. Jderu**, M. Enachescu - „*Matrix of Constraints for the Motion of the Planar Kinematic Chains with Rotational Links with Clearances*", Conference: the 39th American Romanian Academy of Arts and Sciences Congress, 2015. . ISBN: 978-1-4244-4715-2;
6. G. Mihai, C. Moise, A. Pantazi, **A. Jderu**, O. Tutunaru, R. Mesterca, O. Lazar, A. Pumnea, D. Dorobantu, M. Enachescu - „*Optimization of PMMA Processing as a prerequisite for nanodevice building using Electron Beam Litography",* International Conference CHIMIA 2018 „New Trends in Applied Chemestry" – Universitatea Ovidiu din Constanta, 24-26 Mai 2018, Constanta Romania (OP).
7. A. Pandazi, **A. Jderu,** R. Mesterca, G. Mihai, O. Lazar, S. Marin, O. Tutunaru, D. Dorobantu, A. Pumnea, M. Enachescu - „*Adhesive properties studies of f-SWCNTs based nanocomposite thin films",* International Conference CHIMIA 2018 „New Trends in Applied Chemestry" – Universitatea Ovidiu din Constanta, 24-26 Mai 2018, Constanta, Romania (OP).
8. C. Moise, **A. Jderu,** A. Pantazi, R. Mesterca, D. Dorobantu, M. Enachescu - „*Innovative reactor for laser ablation synthesis of carbon nanomaterials"*, European Advanced Materials Congress, EAMC-2018, Stockholm, Sweeden.
9. C. Moise, **A. Jderu,** A. Pantazi, R. Mesterca, D. Dorobantu, M. Enachescu - „*Three Carbon Nanomaterials Synthesized by KrF Laser Ablation in an Innovative Reactor"*, International conference CHIMIA 2018, NOMARES, Constanta, Romania.

10. **A. Jderu,** J. C. Grigore, F. Valeriu, G. Ionescu, M. Enachescu, D. Ziegler - „*Fluids flow measurement using Distributed Calorimetrig Monitoring",* "Mircea cel Batran" Naval Academy, 6th International Scientific Conference SEA-CONF 2020, 22-23 May 2020.
11. **A. Jderu,** D. Bojin, F. Valeriu, G. Ionescu, M. Enachescu, D. Ziegler - „*Distributed Fiber Optical temperature sensig used for mass flow monitoring",* "Mircea cel Batran" Naval Academy, 6th International Scientific Conference SEA-CONF 2020, 22-23 May 2020.
12. **A. Jderu,** J. C. Grigore, I. Popa, D. Bojin, M. Enachescu, D. Ziegler - „*Brillouin Optical Time Domain Analysis technique implementation",* "Mircea cel Batran" Naval Academy, 6th International Scientific Conference SEA-CONF 2020, 22-23 May 2020.
13. D. Dorobantu, **A. Jderu,** G. J. Cristian, G. Ionescu, M. Enachescu, D. Ziegler - „*Optical fibers used for chemical sensing",* "Mircea cel Batran" Naval Academy, 6th International Scientific Conference SEA-CONF 2020, 22-23 May 2020.

Patents:

1. C. Livede, **A. Jderu**, M. Enachescu, I. Popa - „*Metodă și dispozitiv de liniarizare a mișcării actuatoarelor piezoelectrice*", RO131916 (A2) - 2017-05-30, RO20150000687 20150924, H01L41/09; H02N2/06.
2. I. Culeac, M. Enachescu, V. Borsciov, V. Verlan, I. Cojocaru, M. Iovu, **A. Jderu**, D. Dorobantu - „*Sistem și procedeu de pază bazate pe tehnologia cu fibră optică, cu localizarea intervenției neautorizate în sistemul de pază"*, RO133682 (A2) - 2019-10-30, RO20180000807 20181017, G08B13/186, MD1308 (Y) - 2019-01-31, MD1308 (Z) - 2019-08-31.
3. **A. Jderu,** D. Ziegler, M. Enachescu - "*Metodă si dispozitiv pentru monitorizarea calorimetrică a debitului sau fluxului de fluid or masă*", RO134255 (A2) - 2020-06-30, RO20180000823 20181022, G01B9/02; G01F1/66.
4. D. Dorobantu, **A. Jderu,** D. Ziegler, M. Enachescu - "*Metodă de măsurare si dispozitiv de tip senzor pentru detecția chimică cu ajutorul fibrelor optice*". RO135770 (A2) - 2022-05-30, RO20200000744 20201118, G01B11/06; G01N21/77; G02B6/02.